



Deposited via The University of York.

White Rose Research Online URL for this paper:

<https://eprints.whiterose.ac.uk/id/eprint/214336/>

Version: Accepted Version

---

**Article:**

Goldstein, Marvin, Sescu, Adrian and Koshuriyan, Zamir (2012) Effect of non-parallel mean flow on the Green's function for predicting the low frequency sound from turbulent air jets. *Journal of Fluid Mechanics*. 199–234. ISSN: 1469-7645

<https://doi.org/10.1017/jfm.2012.12>

---

**Reuse**

Items deposited in White Rose Research Online are protected by copyright, with all rights reserved unless indicated otherwise. They may be downloaded and/or printed for private study, or other acts as permitted by national copyright laws. The publisher or other rights holders may allow further reproduction and re-use of the full text version. This is indicated by the licence information on the White Rose Research Online record for the item.

**Takedown**

If you consider content in White Rose Research Online to be in breach of UK law, please notify us by emailing [eprints@whiterose.ac.uk](mailto:eprints@whiterose.ac.uk) including the URL of the record and the reason for the withdrawal request.

**Effect of non-parallel mean flow on the Green's function for predicting the low frequency sound from turbulent air jets**

|                               |  |
|-------------------------------|--|
| Journal:                      | <i>Journal of Fluid Mechanics</i>  |
| Manuscript ID:                | JFM-11-S-0582.R1   |
| mss type:                     | Standard   |
| Date Submitted by the Author: | n/a  |
| Complete List of Authors:     | Goldstein, Marvin; National Aeronautics + Space Administration, Glenn Research Center; National Aeronautics + Space Administration, Glenn Research Center<br>Sescu, Adrian; University of Toledo, Mechanical Industrial @ manufacturing Engineering<br>Afsar, Mohammed; OHIO AEROSPACE INSTITUTE |
| Keyword:                      | Aeroacoustics < Acoustics, Jet noise < Acoustics   |
|                               |  |

SCHOLARONE™  
Manuscripts

# Effect of non-parallel mean flow on the Green's function for predicting the low frequency sound from turbulent air jets

By M. E. GOLDSTEIN<sup>1</sup>, ADRIAN SESCOU<sup>2\*</sup> and M. Z. AFSAR<sup>1</sup>

<sup>1</sup>National Aeronautics and Space Administration, Glenn Research Center, Cleveland, OH 44135, USA

<sup>2</sup>University of Toledo, Department of Mechanical Industrial & Manufacturing Engineering, Toledo, OH 43606, USA

\*Current Address Johns Hopkins University, Department of mechanical Engineering, Baltimore MD, 21218, USA

It is now well known that the far-field jet noise spectrum can be expressed as the convolution product of a propagator (that accounts for the mean flow interactions) and a generalized Reynolds stress auto-covariance tensor (that accounts for the turbulence fluctuations). The propagator depends only on the mean flow and an adjoint vector Green's function for a particular form of the linearized Euler equations. Recent numerical calculations (Karabasov, Bogey & Hynes 2011) for a Mach 0.9 jet show that use of the adjoint Green's function for the true non-parallel flow rather than the more conventional locally parallel flow Green's function leads to a significant increase in the predicted low frequency sound radiation at observation angles close to the downstream jet axis. But the non-parallel flow appears to have little effect on the sound radiated at  $90^\circ$  to the downstream axis.

The present paper is concerned with the effects of non-parallel mean flows on the adjoint vector Green's function. We obtain a low frequency asymptotic solution for that function by solving a very simple second order hyperbolic equation for a dependent variable which is directly proportional to pressure-like component of the adjoint Green's function (and roughly corresponds to the strength of a monopole source within the jet). Our numerical calculations show that this quantity remains fairly close to the corresponding parallel flow result at low Mach numbers and that, as expected, it converges to that result when an appropriately scaled frequency parameter is increased. But the convergence occurs at progressively higher frequencies as the Mach number increases and the supersonic solution never actually converges to the parallel flow result in the vicinity of a critical layer singularity that occurs in that solution.

The dominant contribution to the propagator comes from the radial derivative of a certain component of the adjoint vector Green's function. The nonparallel flow has a large effect on this quantity—causing it (and, therefore, the radiated sound) to increase at subsonic speeds and decrease at supersonic speeds. The effects of acoustic source location can be visualized by plotting the magnitude of this quantity, as function of position. These “altitude plots” (which represent the intensity of the radiated sound as a function of source location) show that while the parallel flow solutions exhibit a single peak at subsonic speeds (when the source point is centered on the initial shear layer), the non-parallel solutions exhibit a double peak structure --with the second peak

occurring about two potential core lengths downstream of the nozzle. These results are qualitatively consistent with the numerical calculations reported in Karabasov *et al* (2011).

## INTRODUCTION

There is now a large body of research devoted to jet noise modeling --most of which is based on the acoustic analogy approach developed by Lighthill (1952, 1954, 1963) over 60 years ago. The improved understanding of jet turbulence obtained from experiments and computational studies (e.g. Freund 2003, Harper-Bourne 2003, Pokora & McGuirk 2008, Tam *et al* 2008, McMullen *et al*, 2008, Bodony & Lele 2008; Bogey & Bailly 2010 etc) has resulted in a considerable number of recent developments of Lighthill's original approach. Early developments, such as that of Lilley (1972), which explicitly account for the interaction of the sound with a simplified model of the mean flow, still form the basis of current state-of-the-art jet noise prediction codes (such as the JeNo code; Khavaran, Bridges and Georgiadis 2005, which uses Lilley's formulation along with empirical models for the source terms and Reynolds-averaged Navier-Stokes (RANS) solutions to obtain the mean flow and turbulent kinetic energy).

Goldstein and Leib (hereafter referred to as G&L, see also Goldstein 2003, 201 ) recently used a generalization of the acoustic analogy approach to obtain an exact equation that expresses the far field acoustic spectrum as the product of a propagator (that accounts for the mean flow interactions) and a generalized Reynolds stress auto-covariance tensor (that accounts for the turbulent fluctuations). The propagator only depends on the mean flow and a vector Green's function for a particular form of the linearized Euler equations. But (for reasons given in section 2 below) the present study uses reciprocity to replace the vector Green's function with the corresponding adjoint vector Green's function. G&L used this result to develop an acoustic analogy approach for predicting high-speed jet noise from supersonic jets. They introduced a number of modeling approximations about the mean flow and turbulence in order to reduce the general formula to a form that can be used for practical noise predictions. They assumed --among other things-- that the Strouhal number is  $O(1)$  and the mean flow is weakly non-parallel. Then the non-parallel effects only come into play at supersonic speeds and only affect the solution within a critical layer where the adjoint vector Green's function and, therefore, the propagator become singular. G&L constructed a uniformly valid composite solution for the adjoint Green's function which eliminates the critical-layer singularity that occurs when the observation angle is close to the downstream jet axis.

But it is now realized that non-parallel flow effects can be important at all Mach numbers (Karabasov, Bogey and Hynes, 2011). Karabasov *et al* (2011) show that the non-parallel flow can increase the low frequency radiation from a Mach 0.9 jet by as much as 8 Decibels at small angles to the jet axis but has only an insignificant effect on the sound radiated at  $90^\circ$  to the downstream axis at all frequencies (see their figure 16 parts (a) and(b)). Order of magnitude considerations show that the non parallel flow will have an  $O(1)$  effect on the acoustic spectrum at all Mach numbers when the Strouhal number is of the order of the jet spread rate. The resulting adjoint vector Green's function (and, therefore, the propagator) will then differ from the parallel flow result everywhere

within the jet and not just in the critical layer (as in G&L). It is therefore appropriate to develop an asymptotic formula for the adjoint vector Green's function that is valid in the limit as the spread rate goes to zero while the ratio of the Strouhal number to spread rate remains  $O(1)$ . The present paper shows that this problem can be transformed into one of the two standard boundary value problems for a very simple second order hyperbolic equation (Sokolnikoff & Redheffer, 1958, pp. 504 - 519) for a composite variable, which is denoted by the symbol  $\bar{v}$  and roughly corresponds to the strength of a monopole source within the jet. This remarkably simple result shows, among other things, that 1) the non-parallel flow effects can be lumped into a single coefficient that is related to the mean flow advection vector, that 2) the composite variable  $\bar{v}$  is fairly close to the corresponding parallel flow result at low Mach numbers and that 3) it converges to this solution as an appropriate scaled frequency parameter increases. But it also shows that the convergence occurs at progressively higher frequencies as the Mach number increases and that the supersonic solution never converges to this result in the vicinity of a critical layer singularity that occurs in the parallel flow solution (see G & L).

At supersonic speeds, the primary nonparallel flow effect is the elimination of a critical layer singularity that occurs in the parallel flow model, which results in reduction in the predicted level of acoustic radiation. The present analysis shows that the nonparallel effects increase the low frequency sound at subsonic Mach numbers, as found by Karabasov *et al* (2011) and Karabasov *et al* (2010), but, as noted above, have the opposite effect at supersonic speeds. And while the effects are much larger at supersonic Mach numbers, they are still quite significant at subsonic speeds. The dominant contribution to the propagator comes from the radial derivative of a certain component of the Fourier transformed adjoint vector Green's function. The nonparallel effects cause this quantity (and, therefore, the radiated sound) to increase at subsonic speeds and decrease at supersonic speeds. The effects of source location can be visualized by plotting the magnitude of this quantity as function of position. These "altitude plots" (which represent the intensity of the radiated sound as a function of source location) show that while the parallel flow solutions exhibit a single peak at subsonic speeds (when the acoustic source is centered on the initial shear layer), the non-parallel solutions exhibit a double peak structure with the second peak occurring on the nozzle lip line about two potential core lengths downstream (where the turbulence level is still relatively high). The resulting acoustic waves are probably of the conventional spherically spreading type and may differ from the lateral head waves considered by Howe (1970) in the low frequency limit and by Suzuki and Lele (2003) in the high frequency limit.

The calculations show that the deviations between the parallel and non-parallel flow results are much larger for the radial derivative of the streamwise component of the Green's function than they are for composite dependent variable  $\bar{v}$  that was introduced to simplify the equations. These results are consistent with the Karabasov *et al* (2011) numerical computations, which show that the largest increase in low frequency sound occurs when the source is about two potential core lengths downstream from the nozzle. The present asymptotic approach provides considerable insight into the relevant physics and is expected to be complimentary to the numerical computations of Karabasov *et al* (2010, 2011). The results are also of interest from the point of view of classical

acoustics. They show, among other things, how vortical disturbances in the vicinity of the physical source point  $\mathbf{y}$  evolve into irrotational acoustic wave as they propagate into the far field.

The role played by the adjoint vector Green's function in the exact formula for the acoustic radiation from a turbulent air jet is set out in section 2. The asymptotic representation for the slowly diverging mean flow is discussed in section 3. Appropriate far field boundary conditions are derived for the adjoint Green's function in section 4.1 and its low frequency limit is described in section 4.2. The general results of that section are applied to a round jet in section 5 where the boundary value problem for the low frequency solution is transformed into a much simpler problem for a second order hyperbolic partial differential equation--which is then solved by the numerical procedure described in section 6. The results are presented and analyzed in section 7.

## 2. Basic Context

The pressure  $p$ , density  $\rho$ , enthalpy  $h$  and speed of sound  $c$  are assumed to satisfy the ideal gas law equation of state

$$p = \rho c^2 / \gamma, \quad h = c^2 / (\gamma - 1) \quad (2.1)$$

where  $\gamma$  denotes the specific heat ratio. It is customary to express the Fourier transform

$$I_\omega(\mathbf{x}) \equiv \frac{1}{2\pi} \int_{-\infty}^{\infty} e^{i\omega\tau} \overline{p'(\mathbf{x}, t) p'(\mathbf{x}, t + \tau)} d\tau, \quad (2.2)$$

of the far-field pressure autocovariance  $\overline{p'(\mathbf{x}, t) p'(\mathbf{x}, t + \tau)}$ -- usually referred to as the acoustic spectrum at the observation point  $\mathbf{x} = \{x_1, x_2, x_3\}$  in terms of  $I_\omega(\mathbf{x} | \mathbf{y})$ , the acoustic spectrum at  $\mathbf{x}$  due to a unit volume of turbulence at  $\mathbf{y} = \{y_1, y_2, y_3\}$ , by

$$I_\omega(\mathbf{x}) = \int_V I_\omega(\mathbf{x} | \mathbf{y}) d\mathbf{y}, \quad (2.3)$$

where the integration volume,  $V$ , is the entire source region,  $p' \equiv p - \bar{p}$  and over-bars are being used to denote time averages. G & L show that this latter quantity is given by

$$I_\omega(\mathbf{x} | \mathbf{y}) = (2\pi)^2 \Gamma_{\lambda j}(\mathbf{x} | \mathbf{y}; \omega) \int_V \Gamma_{\kappa l}^*(\mathbf{x} | \mathbf{y} + \boldsymbol{\eta}; \omega) \mathcal{N}_{\lambda j \kappa l}(\mathbf{y}, \boldsymbol{\eta}, \omega) d\boldsymbol{\eta} \quad (2.4)$$

where the asterisk denotes complex conjugates, the the Einstein summation convention is being used with the Greek indices ranging from one to four and the Latin indices from one to three.

$$\Gamma_{\lambda j}(\mathbf{x} | \mathbf{y}; \omega) \equiv \frac{\partial G_\lambda(\mathbf{y} | \mathbf{x}; \omega)}{\partial y_j} - (\gamma - 1) \delta_{\lambda k} \frac{\partial \tilde{v}_k}{\partial y_j} G_4(\mathbf{y} | \mathbf{x}; \omega) \quad (2.5)$$

is a "propagator" that depends on the mean flow and the Fourier transform

$$G_\lambda(\mathbf{y}|\mathbf{x};\omega) \equiv \frac{1}{2\pi} \int_{-\infty}^{\infty} e^{i\omega(t-\tau)} g_{\lambda 4}^a(\mathbf{y}, \tau|\mathbf{x}, t) d(t-\tau) \quad (2.6)$$

of the 4<sup>th</sup> fourth component adjoint vector Green's function  $g_{v4}^a(\mathbf{y}, \tau|\mathbf{x}, t)$ ,  $v = 1, 2, \dots, 5$  for the linearized Euler operators that appear on the left sides of the five Generalized acoustic analogy equations (See equations (2.18)-(2.20) and equations (3.1)-(3.3) of G & L and pp. 878-886 of Morse and Feshbach, 1953). It is related to the 4<sup>th</sup> component of the ordinary vector Green's function  $g_{4v}(\mathbf{x}, t|\mathbf{y}, \tau)$  by the reciprocity relation

$$g_{v4}^a(\mathbf{y}, \tau|\mathbf{x}, t) = g_{4v}(\mathbf{x}, t|\mathbf{y}, \tau) \quad (2.7)$$

and satisfies the adjoint equations (See equations (4.8)-(2.10) of G & L)

$$-\frac{\tilde{D}g_{i4}^a}{D\tau} + g_{j4}^a \frac{\partial \tilde{v}_j}{\partial y_i} - \tilde{c}^2 \frac{\partial g_{44}^a}{\partial y_i} + (\gamma - 1) X_i g_{44}^a - \frac{\partial g_{54}^a}{\partial y_i} = 0 \quad (2.8)$$

$$-\frac{\tilde{D}g_{44}^a}{D\tau} - \frac{\partial g_{i4}^a}{\partial y_i} + (\gamma - 1) g_{44}^a \frac{\partial \tilde{v}_j}{\partial y_j} = \delta(\mathbf{x} - \mathbf{y}) \delta(t - \tau) \quad (2.9)$$

$$-\frac{\tilde{D}g_{54}^a}{D\tau} + X_i g_{i4}^a = 0 \quad (2.10)$$

where the tilde denotes the Favre-average

$$\tilde{\bullet} \equiv (\overline{\rho \bullet} / \bar{\rho}) \quad (2.11)$$

of any flow quantity  $v_k$  denotes the flow velocity,

$$\tilde{c}^2 \equiv \gamma \bar{p} / \bar{\rho} \quad (2.12)$$

denotes the mean flow sound speed squared,

$$\frac{\tilde{D}}{D\tau} \equiv \frac{\partial}{\partial \tau} + \tilde{v}_i(\mathbf{y}, \tau) \frac{\partial}{\partial y_i} \quad (2.13)$$

denotes the mean flow convective derivative and

$$X_i \equiv \frac{\tilde{D}}{D\tau} \tilde{v}_i \quad (2.14)$$

denotes the mean flow advection vector.

As usual, the first two arguments of the Green's functions  $g_{4v}(\mathbf{x}, t|\mathbf{y}, \tau)$  and  $g_{v4}^a(\mathbf{y}, \tau|\mathbf{x}, t)$  refer to the independent variables in the relevant Green's function equations and the second two arguments correspond to the space/time source point. The subscript  $v$  is associated with the components of the linearized Euler operators that appear on the left side of the generalized acoustic

analogy equations (equations (2.18)-(2.20) of G & L). The reciprocity relation (2.7) shows that the dependent variable  $\mathbf{y}$  in the adjoint Green's function  $g_{v4}^a(\mathbf{y}, \tau | \mathbf{x}, t)$  corresponds to the actual physical source point while the source variable  $\mathbf{x}$  corresponds to the actual "observation point". Equation (2.7) and the physical equations (equations (2.18)-(2.20) of G & L) also show that the  $g_{44}^a(\mathbf{y}, \tau | \mathbf{x}, t)$  component of  $g_{v4}^a$  can be associated with the pressure fluctuations but the remaining components have no direct physical significance-though (2.10) suggests that  $g_{54}^a(\mathbf{y}, \tau | \mathbf{x}, t)$  can be associated with the convected component of the motion since  $X_i = 0$  in a strictly parallel flow. The adjoint linearized Euler equations (A 6)-(A 8) of Tam and Auriault (1998) can be transformed into equations (2.8)-(2.10) by using the steady (non-linear) Euler equations to rearrange their coefficients. But these equations can only be compatible with the exact generalized acoustic analogy equations (equations (2.18)-(2.20) of G & L) when they are written in the form (2.8)-(2.10).

Tam and Auriault (1998) argue that the adjoint Green's function is preferable to the direct Green's function because it simplifies the numerical computations. But we use it here because it allows the far field expansion to be carried out before the governing equations are solved and, thereby, greatly simplifies the analysis (by removing the delta function from the right hand side of the governing equations). It also greatly reduces the number of equations that have to be solved (the direct Green's function can only be found by solving  $25=5 \times 5$  equations) and simplifies the formulation of the far field boundary conditions (see section 3. below). These technical considerations have no effect on the final results because the 4-4 pressure like components of the two Green's functions are simply related the reciprocity relation (2.7)

The tensor  $\mathcal{R}_{\lambda j \kappa l}$ ,  $j, l = 1, 2, 3$ ;  $\lambda, \kappa = 1, 2, 3, 4$  accounts for the turbulent velocity and enthalpy fluctuations in the jet and has to be modeled in the acoustic analogy approach. It is related (by the simple linear transformation (5.13) of G & L) to the spectrum of a generalized Reynolds stress autocovariance tensor given explicitly by equation (5.12) of G & L in the absence of viscous effects. But these formulas are irrelevant for the purposes of this paper which focuses on the mean flow interaction effects.

Equation (2.4) and (2.5) provide an (essentially) exact relation between the quantities that are typically measured in Aeroacoustics experiments, namely the far-field acoustic spectrum and the generalized Reynolds stress autocovariance tensor (equation (5.12) of G & L). They are identical to equations (5.13) and (5.14) of G & L rewritten in terms of the fixed frame separation vector, i.e. with the artificially introduced convection velocity  $U_c$  set equal to zero in equations (5.10) and (5.14) of G & L--so that  $\boldsymbol{\xi} = \boldsymbol{\eta}$  in (5.14). They are completely general and apply to any localized turbulent flow, even in the presence of fixed solid surfaces, say  $S = S(\mathbf{y})$ , as long as  $g_{\lambda 4}^a(\mathbf{y}, \tau | \mathbf{x}, t)$  is assumed to satisfy

$$\hat{n}_i g_{i4}^a(\mathbf{y}, \tau | \mathbf{x}, t) = 0 \quad \text{for } \mathbf{y} \text{ on } S \quad (2.15)$$

where  $\hat{n}_i$  denotes the unit normal to  $S$ .

### 3. The mean flow expansion

As usual we suppose that all lengths have been scaled with a characteristic nozzle radius  $r_j$ , all velocities by the mean jet exit velocity  $U_j$  etc.. The mean flow is assumed to have small spread rate, say  $\varepsilon$ , and to vary on the slow streamwise length scale

$$Y \equiv \varepsilon y_1 \quad (3.1)$$

It is, therefore, expected to expand like (see equations 5.1 & 5.2 of G & L)

$$\tilde{\mathbf{v}} = \{U(Y, \mathbf{y}_T), \varepsilon \mathbf{V}_T(Y, \mathbf{y}_T)\} + \varepsilon \{U^{(1)}(Y, \mathbf{y}_T), \varepsilon \mathbf{V}_T^{(1)}(Y, \mathbf{y}_T)\} + \dots \quad (3.2)$$

$$\begin{aligned} \bar{\rho} &= \bar{\rho}(Y, \mathbf{y}_T) + \varepsilon \bar{\rho}^{(1)}(Y, \mathbf{y}_T) + \dots, & \tilde{c}^2 &= \tilde{c}^2(Y, \mathbf{y}_T) + \varepsilon (\tilde{c}^2)^{(1)}(Y, \mathbf{y}_T) + \dots, \\ & & \bar{p} &= \text{const} + \varepsilon \bar{p}^{(1)}(Y, \mathbf{y}_T) + \dots \end{aligned} \quad (3.3)$$

$$\mathbf{X} = \{\varepsilon \bar{X}_1, \varepsilon^2 \bar{X}_T\} + \varepsilon \{\varepsilon \bar{X}_1^{(1)}, \varepsilon^2 \bar{X}_T^{(1)}\} + \dots \quad (3.4)$$

in an inner region, where the magnitude

$$r \equiv |\mathbf{y}_T| = \sqrt{y_2^2 + y_3^2} \quad (3.5)$$

of the transverse coordinate  $\mathbf{y}_T = \{y_2, y_3\}$  is  $O(1)$ . This expansion will break down in an outer region where the scaled transverse coordinate

$$R \equiv \varepsilon r \quad (3.6)$$

is  $O(1)$  when the scaled transverse velocity  $\tilde{\mathbf{V}}_T = \{\tilde{V}_2, \tilde{V}_3\}$  decays like  $|\mathbf{y}_T|^{-1}$  as  $\mathbf{y}_T = \{y_2, y_3\} \rightarrow \infty$ .

However, the mean flow velocity will then be  $O(\varepsilon^2)$  in this region and will not affect the Green's function solution to the order of approximation of the analysis.

But the higher order terms in the expansion (3.2)-(3.4) will produce inhomogeneous terms in the  $n=1$  Green's function equations (5.9)-(5.13) derived in section 5 below. However, the resulting inhomogeneous solution to these equations will, for reasons given in that section, only make a higher order contribution to the inner expansion (5.5) and (5.6) of the adjoint vector Green's function. These higher order terms will, therefore, be omitted since their inclusion would significantly complicate the equations.

## 4. The Green's function Solution

### 4.1 The Far Field

In order to take advantage of the simplification that occurs when the observation point  $\mathbf{x}$  is in the far field, we begin by considering the far field region where  $\mathbf{x}, \mathbf{y} \rightarrow \infty$ . Then

$\tilde{v}_k \rightarrow 0, \tilde{c}^2 \rightarrow c_\infty^2 = \text{constant}$  and equations (2.8)-(2.10) become

$$-\frac{\partial g_{i4}^a}{\partial \tau} - c_\infty^2 \frac{\partial g_{44}^a}{\partial y_i} = 0 \quad (4.1)$$

$$-\frac{\partial g_{44}^a}{\partial \tau} - \frac{\partial g_{i4}^a}{\partial y_i} = \delta(\mathbf{x} - \mathbf{y}) \delta(t - \tau) \quad (4.2)$$

$$-\frac{\partial g_{54}^a}{\partial \tau} = 0 \quad (4.3)$$

to within an error of  $O(\varepsilon^2)$ . It, therefore, follows that  $g_{44}^a$  satisfies the inhomogeneous wave equation

$$-\frac{\partial^2 g_{44}^a}{\partial \tau^2} + c_\infty^2 \frac{\partial^2 g_{44}^a}{\partial y_i \partial y_i} = \delta(\mathbf{x} - \mathbf{y}) \frac{\partial}{\partial \tau} \delta(t - \tau) \quad (4.4)$$

The relevant solution satisfies the causality condition

$$g_{44}^a(\mathbf{y}, \tau | \mathbf{x}, t) = 0 \text{ for } t < \tau \quad (4.5)$$

and is given by (Goldstein, 2006, Appendix A)

$$g_{44}^a(\mathbf{y}, \tau | \mathbf{x}, t) = \frac{-1}{4\pi |\mathbf{x} - \mathbf{y}| c_\infty^2} \frac{\partial}{\partial \tau} \delta\left(\tau - t + \frac{|\mathbf{x} - \mathbf{y}|}{c_\infty}\right) \quad (4.6)$$

plus reflected and scattered waves generated by the mean flow and solid surface interactions. It follows that

$$g_{44}^a \rightarrow \frac{-1}{4\pi x c_\infty^2} \frac{\partial}{\partial \tau} \delta\left(\tau - \frac{\mathbf{x} \cdot \mathbf{y}}{x c_\infty} - t + \frac{x}{c_\infty}\right) \quad (4.7)$$

when  $x \equiv |\mathbf{x}| \rightarrow \infty$  which becomes

$$G_4(\mathbf{y} | \mathbf{x}; \omega) \rightarrow -\frac{i\omega}{x^2 (2\pi c_\infty)^2} e^{i\omega x/c_\infty - i\omega \mathbf{y} \cdot \mathbf{x}/x c_\infty} \quad (4.8)$$

upon taking the Fourier transform  $G_4(\mathbf{y} | \mathbf{x}; \omega)$  defined by

$$G_i(\mathbf{y}, \omega) \equiv \int_{-\infty}^{\infty} e^{i\omega(\tau-t)} g_{i4}(\mathbf{y}, \tau | \mathbf{x}, t) d(\tau-t) \quad i=1,2,3,4 \quad (4.9)$$

It, therefore, follows from equations(2.15), (4.1) and (4.4) that

$$G_4(\mathbf{y} | \mathbf{x}; \omega) \rightarrow -\frac{i\omega}{x^2 (2\pi c_\infty)^2} e^{i\omega x/c_\infty} \left[ e^{-i\omega \mathbf{y} \cdot \mathbf{x}/x c_\infty} + \Phi(\mathbf{y}, \omega | \mathbf{x} / x) \right] \quad (4.10)$$

for  $|\mathbf{x}| \rightarrow \infty$  and  $|\mathbf{y}| \gg 1$

when the jet and nozzle are explicitly accounted for. The function  $\Phi$  represents an outgoing disturbance that satisfies the Fourier transformed wave equation

$$\omega^2 \Phi + c_\infty^2 \frac{\partial^2 \Phi}{\partial y_i \partial y_i} = 0 \quad (4.11)$$

together with the boundary condition

$$\hat{n}_i \frac{\partial}{\partial y_i} e^{-i\omega \mathbf{y} \cdot \mathbf{x}/x c_\infty} + \hat{n}_i \frac{\partial \Phi(\mathbf{y}, \omega | \mathbf{x} / x)}{\partial y_i} = 0 \quad \mathbf{y} \text{ on } S \quad (4.12)$$

on the nozzle surface  $S$ .

## 4.2 Low Frequency Solution (Distinguished limit)

As noted in the introduction, G & L showed that the nonparallel flow can only have an  $O(1)$  effect on the Green's function solution within a narrow critical layer at  $O(1)$  frequencies. But the present analysis will show that it can change the leading order behavior of the Green's function everywhere in the flow at sufficiently low frequencies or equivalently when the variations in time are sufficiently slow. This occurs when the time variations are of the same order as the streamwise variations in the mean flow, i.e. when they take place on the slow time scale

$$\tilde{T} \equiv \varepsilon \tau \quad (4.13)$$

or equivalently when the scaled frequency  $\omega$  (or Strouhal number) is of the order of the jet spread rate  $\varepsilon$ . The distinguished scaling corresponds to the limit where the mean flow spread rate  $\varepsilon$  goes to zero with the scaled frequency

$$\Omega \equiv \omega / \varepsilon = O(1) \quad (4.14)$$

held fixed. Then the Green's function solution, like the steady flow solution described in section 4.1, will divide into an inner solution in the region where the transverse  $r \equiv |\mathbf{y}_T|$  given by equation (3.5) is of  $O(1)$  and an outer solution in the region where the scaled transverse coordinate  $R$  defined by equation (3.6) is  $O(1)$  and the Fourier transformed Green's function is given by (4.10) when the observation point  $\mathbf{x}$  is in the far field.

The outer boundary condition for the inner solution is obtained by requiring that it match onto the inner expansion of the outer solution (4.10) (Van Dyke, 1975, Chapter III). So rewriting (4.10) in terms of the outer variables  $(Y, R)$  shows that  $G_4$  must satisfy the boundary condition

$$G_4(\mathbf{y}|\mathbf{x}; \omega) \rightarrow -\frac{i\omega}{x^2(2\pi c_\infty)^2} e^{i\omega x/c_\infty} \underset{\text{as } R \rightarrow 0}{\text{inner exp.}} \left\{ e^{-i\Omega[Y \cos\theta + R \sin\theta \cos(\varphi - \tilde{\varphi})]/c_\infty} \right. \\ \left. + \tilde{\Phi}(Y, \mathbf{Y}_T, \Omega, \varepsilon | \theta, \varphi - \tilde{\varphi}) \right\} \\ \text{as } r \equiv |\mathbf{y}_T| \rightarrow \infty \text{ with } Y \geq 0 \quad (4.15)$$

where "inner exp." denotes the inner expansion of the term in curly brackets,  $Y$  is defined by (3.1),  $\theta \equiv \cos^{-1} x_1/x$  denotes the polar observation angle measured from the downstream jet axis,  $\varphi$  and

$$\tilde{\varphi} = \tan^{-1}(y_2/y_3) \quad (4.16)$$

denote azimuthal angles of the observation and source points respectively,  $\mathbf{Y}_T = \{Y_2, Y_3\} \equiv \varepsilon \mathbf{y}_T$  and  $\tilde{\Phi}(Y, \mathbf{Y}_T, \Omega, \varepsilon | \theta, \varphi - \tilde{\varphi})$  denotes the outgoing disturbance  $\Phi(\mathbf{y}, \omega | \mathbf{x}/x)$  rewritten in terms of the outer variables.

Rewriting the boundary condition (4.12) in terms of the inner variables  $(Y, R)$  shows that

$$\varepsilon \hat{n}_i \frac{\partial}{\partial Y_i} e^{-i\Omega R \sin\theta \cos(\varphi - \tilde{\varphi})/c_\infty} + \hat{n}_i \frac{\partial \Phi(\mathbf{y}, \omega | \mathbf{x}/x)}{\partial y_i} = 0$$

$$\text{for } Y < 0, \mathbf{y}_T \text{ on solid surface,} \quad (4.17)$$

where  $\hat{\mathbf{n}} = \hat{\mathbf{n}}(\mathbf{y})$  denotes the outward drawn normal to the upstream nozzle surface, which will have  $O(r_j)$  transverse dimensions and which is assumed, for simplicity, to be parallel to the  $y_1$ -direction. These results can be made more explicit by restricting them to the important case of a (non-swirling) round jet for which the mean flow is independent of  $\tilde{\varphi}$  and the circumferential velocity is zero.

## 5. Round Jet

The outgoing wave  $\tilde{\Phi}$  in (4.15) can then be written more explicitly as

$$\tilde{\Phi}(Y, Y_T, \Omega, \varepsilon | \theta, \varphi - \tilde{\varphi}) = \sum_{n=-\infty}^{\infty} e^{in(\varphi - \tilde{\varphi})} \Phi_n(Y, R, \Omega, \varepsilon | \theta) \quad (5.1)$$

where

$$\Phi_n(Y, R, \Omega, \varepsilon | \theta) \equiv \int_{-\infty}^{\infty} e^{-iKY} C_n(K, \Omega, \varepsilon | \theta) H_n^{(1)}\left(R\sqrt{K^2 - (\Omega/c_\infty)^2}\right) dK \quad (5.2)$$

and  $H_n^{(1)}$  denotes the Hankel function in the usual notation (Abramowitz & Stegun, 1965, p.360).

Then since (Abramowitz & Stegun, 1965, pp.375 & 376)

$$\int_{-\pi}^{\pi} e^{i\varepsilon\Omega/c_\infty \sin\theta r \cos(\varphi - \tilde{\varphi}) + in(\varphi - \tilde{\varphi})} d(\varphi - \tilde{\varphi}) = 2\pi e^{-in\pi/2} J_n\left(\frac{\Omega}{c_\infty} \varepsilon \sin\theta r\right), \quad (5.3)$$

where  $J_n$  denotes the Bessel function in the usual notation, it follows from (4.15), (5.1) and the series expansion for the Bessel function that

$G_4 \rightarrow$

$$-i\Omega \sum_{n=-\infty}^{\infty} e^{in(\varphi - \tilde{\varphi}) - in\pi/2} \left[ e^{-i\Omega Y \cos\theta/c_\infty} \frac{1}{n!} (\varepsilon r \Omega \sin\theta/c_\infty)^n (1 + O(\varepsilon r)^2) \right. \\ \left. + \text{inner expansion of } \Phi_n(Y, R, \Omega, \varepsilon | \theta) \text{ re-expressed in terms of inner variable } r \right] \quad (5.4)$$

as  $r \rightarrow \infty$  with  $Y \geq 0$

And since the inner solution, is induced by the incoming waves represented by the leading terms in the square brackets, while the  $\Phi_n$  represent the outgoing waves generated by (i.e., forced by) that solution, and since this equation and the mean flow equations (3.2)–(3.4) both depend on  $y_1$  only through the slow streamwise variable  $Y$ , the dominant balance in the inner region,  $\mathbf{y}_T = O(1)$ , must be (Van Dyke, 1975, p.30)

$$g_{i4}^a(\mathbf{y}, \tau | \mathbf{x}, t) = g_{i4}^{(0)}(Y, r, \tilde{\varphi}, \tilde{T} | \mathbf{X}, T) + \varepsilon g_{i4}^{(1)}(Y, r, \tilde{\varphi}, \tilde{T} | \mathbf{X}, T) + \dots, \quad i = 1, 4, 5 \quad (5.5)$$

$$\mathbf{g}_{T4}^a(\mathbf{y}, \tau | \mathbf{x}, t) = \{g_{r4}^a, g_{\tilde{\varphi}4}^a\} = \varepsilon^{-1} \mathbf{g}_{T4}^{(0)}(Y, r, \tilde{\varphi}, \tilde{T} | \mathbf{X}, T) + \mathbf{g}_{T4}^{(1)}(Y, r, \tilde{\varphi}, \tilde{T} | \mathbf{X}, T) + \dots \quad (5.6)$$

where the slow time variable  $\tilde{T}$  is defined by (4.13) and  $r, \tilde{\varphi}$  are the cylindrical coordinates defined in (3.5) and (4.16). Since it follows from (5.2) that (see Abramowitz & Stegun, 1965, p.360)

$$\Phi_0(Y, R, \Omega, 0 | \theta) \rightarrow f(Y, \Omega, |\theta) \ln R \quad \text{as } R \rightarrow 0 \quad (5.7)$$

the expansion (5.5) and (5.6) would also contain logarithmic terms if the function  $f$  were not equal to zero, but these terms are omitted since  $\Phi_0$  is induced by the inner solution and would only be non-zero if  $g_{i4}^{(0)}$  were to behave like  $\ln r$  as  $r \rightarrow \infty$ , which, as shown below, would not be consistent with the governing equations.

Substituting these expansions into (2.8)–(2.10) and (4.15) rewritten in terms of the cylindrical coordinates (3.5) and (4.16) (See equations (21 a)–(21 b) of Tam and Auriault, 1998) and noting that the result depends on  $T$  and  $\tilde{T}$  only in the combination  $T - \tilde{T}$  shows that the scaled Fourier transforms

$$\frac{\varepsilon}{x^2 (2\pi c_\infty)^2} e^{i\Omega X/c_\infty} G_\kappa^{(n)}(Y, \mathbf{y}_T, \Omega) \equiv \frac{1}{2\pi\varepsilon} \int_{-\infty}^{\infty} e^{i\Omega(T-T_0)} g_{\kappa 4}^{(n)}(Y, \mathbf{y}_T, T_0 | \mathbf{X}, T) d(T - T_0), \quad (5.8)$$

$$n = 0, 1: \quad \kappa = 1, 4, 5, r, \tilde{\varphi}$$

satisfy

$$-D_0 G_1^{(n)} + G_1^{(n)} \frac{\partial U}{\partial Y} + G_r^{(n)} \frac{\partial V_r}{\partial Y} - \tilde{c}^2 \frac{\partial G_4^{(n)}}{\partial Y} + (\gamma - 1) \bar{X}_1 G_4^{(n)} - \frac{\partial G_5^{(n)}}{\partial Y} = 0 \quad (5.9)$$

$$-D_0 G_r^{(n)} + G_1^{(n)} \frac{\partial U}{\partial r} + G_r^{(n)} \frac{\partial V_r}{\partial r} - \tilde{c}^2 \frac{\partial G_4^{(n)}}{\partial r} - \frac{\partial G_5^{(n)}}{\partial r} = 0 \quad (5.10)$$

$$-D_0 G_{\tilde{\varphi}}^{(n)} - \frac{G_{\tilde{\varphi}}^{(n)} V_r}{r} - \tilde{c}^2 \frac{1}{r} \frac{\partial G_4^{(n)}}{\partial \tilde{\varphi}} - \frac{1}{r} \frac{\partial G_5^{(n)}}{\partial \tilde{\varphi}} = 0 \quad (5.11)$$

$$\frac{\partial r G_r^{(n)}}{\partial r} + \frac{\partial G_{\tilde{\varphi}}^{(n)}}{\partial \tilde{\varphi}} = 0 \quad (5.12)$$

$$-D_0 G_5^{(n)} + \bar{X}_1 G_1^{(n)} + \bar{X}_r G_r^{(n)} = 0 \quad (5.13)$$

where  $n = 0, 1$ ,

$$D_0 \equiv i\Omega + U \frac{\partial}{\partial Y} + V_r \frac{\partial}{\partial r} \quad (5.14)$$

and

$$\bar{X}_1 \equiv \left( U \frac{\partial}{\partial Y} + V_r \frac{\partial}{\partial r} \right) U, \quad \bar{X}_r \equiv \left( U \frac{\partial}{\partial Y} + V_r \frac{\partial}{\partial r} \right) V_r \quad (5.15)$$

Then since, as noted above, the  $\Phi_n$  represent the outgoing waves generated by (i.e., forced by) the inner solution, which is induced by the incoming waves represented by the leading terms in the square brackets of (5.2), the  $G_i^{(0)}$  must be axisymmetric and (5.5), (5.8) and (5.4), therefore, imply that (see (Abramowitz & Stegun, 1965, p.360)

$$G_i^{(0)} + \varepsilon G_i^{(1)} + \dots = G_i^{(0)}(r, Y) - \varepsilon \cos(\varphi - \tilde{\varphi}) \tilde{G}_i^{(1)}(r, Y) + \dots, \quad i = 1, r, 4, 5 \quad (5.16)$$

$$G_{\tilde{\varphi}}^{(0)} + \varepsilon G_{\tilde{\varphi}}^{(1)} + \dots = \tilde{G}_{\tilde{\varphi}}^{(0)}(r, Y) + \varepsilon \sin(\varphi - \tilde{\varphi}) \tilde{G}_{\tilde{\varphi}}^{(1)}(r, Y) + \dots$$

So equations (5.11) and (5.12) with  $n = 0$  show that

$$G_r^{(0)} = G_{\tilde{\varphi}}^{(0)} = 0 \quad (5.17)$$

since  $G_r^{(0)}$  must be finite and  $G_{\tilde{\varphi}}^{(0)}$  must be zero at  $r = 0$ , and equations (5.9), (5.10), and (5.13) become

$$-D_0 G_1^{(0)} + G_1^{(0)} \frac{\partial U}{\partial Y} - \tilde{c}^2 \frac{\partial G_4^{(0)}}{\partial Y} + (\gamma - 1) \bar{X}_1 G_4^{(0)} - \frac{\partial G_5^{(0)}}{\partial Y} = 0 \quad (5.18)$$

$$G_1^{(0)} \frac{\partial U}{\partial r} - \tilde{c}^2 \frac{\partial G_4^{(0)}}{\partial r} - \frac{\partial G_5^{(0)}}{\partial r} = 0 \quad (5.19)$$

$$-D_0 G_5^{(0)} + \bar{X}_1 G_1^{(0)} = 0 \quad (5.20)$$

Since equations (5.8) and (5.17) show that the lowest order  $\mathbf{g}_{T_4}^{(0)}$ -term is zero in (5.6) while the expansion (5.16) implies that the  $\mathbf{g}_{T_4}^{(1)}$ -term (which is of the same order as the  $\mathbf{g}_{i_4}^{(0)}$  terms in (5.5)) will be non-zero, the contribution of the higher order non-axisymmetric  $G_{\kappa}^{(1)}$ ,  $\kappa = r, \tilde{\varphi}$  terms to the total Green's function will, be  $O(1)$ , i.e. of the same order as the lower order  $G_i^{(0)}$  terms. Retention of the higher order terms in the mean flow expansion (3.2)- (3.4) would, as noted above, have produced inhomogeneous terms in the  $n=1$  equations (5.9)-(5.13). But these terms would be proportional to  $G_{\kappa}^{(0)}(r, \Omega)$  and would, therefore, be axisymmetric (i.e. independent  $\tilde{\varphi}$ ), which means that their net effect would be to produce an  $O(\varepsilon)$  axisymmetric contribution to the expansion (5.16), and, therefore, an  $O(\varepsilon)$  correction to the  $O(1)$  terms in the expansions (5.5) and (5.6). These terms can, therefore, be neglected and the omission of the higher order terms in the mean flow expansion (3.2)-(3.4) is, therefore, justified.

But the calculations of Karabasov *et al* (2011) and Karabasov *et al* (2010) show that the non parallel flow effects only come into play at relatively small observation angles where (as shown by Goldstein (1975) and Afsar (2010) for a strictly parallel mean flow and by Karabasov *et al* (2007, see figure (14a)) for a non-parallel flow) the axisymmetric term makes the dominant contribution. It is, therefore, appropriate to only consider the  $n=0$  solution.

Equations (5.18)-(5.20) can be greatly simplified by taking  $U$  and  $Y$  to be the independent variables and using the chain rule along with (5.15) to rewrite equation (5.14) as

$$D_0 \tilde{G}_i \equiv \left( \bar{D}_0 + \bar{X}_1 \frac{\partial}{\partial U} \right) \tilde{G}_i = \left( i\Omega + U \frac{\partial}{\partial Y} + \bar{X}_1 \frac{\partial}{\partial U} \right) \tilde{G}_i = \left( i\Omega + U \frac{\partial}{\partial Y} + V_r \frac{\partial}{\partial r} \right) G_i^{(0)} \quad (5.21)$$

where  $\bar{D}_0$  is defined by the second member of this equation and  $\tilde{G}_i = \tilde{G}_i(U, Y)$  is defined implicitly in terms of  $G_i^{(0)}(r, Y)$  by

$$\tilde{G}_i(U(r, Y), Y) = G_i^{(0)}(r, Y) \quad (5.22)$$

The partial derivative with respect to  $Y$  is at constant  $U$  in the third member and at constant  $r$  in the last member. It then follows from (5.19) that

$$\tilde{G}_1 = \tilde{c}^2 \frac{\partial \tilde{G}_4}{\partial U} + \frac{\partial \tilde{G}_5}{\partial U} \quad (5.23)$$

Applying the chain rule to (5.18), therefore, shows that

$$-D_0 \tilde{G}_1 - \tilde{c}^2 \frac{\partial \tilde{G}_4}{\partial Y} - \frac{\partial \tilde{G}_5}{\partial Y} + (\gamma - 1) \bar{X}_1 \tilde{G}_4 = 0 \quad (5.24)$$

and equation (5.20) can be written as

$$-\bar{D}_0 \tilde{G}_5 + \bar{X}_1 \tilde{c}^2 \frac{\partial \tilde{G}_4}{\partial U} = 0 \quad (5.25)$$

which means that

$$\bar{D}_0 \bar{v} = \tilde{c}^2 D_0 \tilde{G}_4 \quad (5.26)$$

and

$$\tilde{G}_1 = -\tilde{G}_4 \frac{\partial \tilde{c}^2}{\partial U} + \frac{\partial \bar{v}}{\partial U} \quad (5.27)$$

where

$$\bar{v} \equiv \tilde{c}^2 \tilde{G}_4 + \tilde{G}_5 \quad (5.28)$$

and  $\bar{D}_0$  is implicitly defined by (5.21). Equation (5.24) then becomes

$$-D_0 \left( \frac{\partial \bar{v}}{\partial U} - \tilde{G}_4 \frac{\partial \tilde{c}^2}{\partial U} \right) - \tilde{c}^2 \frac{\partial \tilde{G}_4}{\partial Y} - \frac{\partial \tilde{G}_5}{\partial Y} + (\gamma - 1) \bar{X}_1 \tilde{G}_4 = 0 \quad (5.29)$$

which can be written as

$$-\frac{\partial}{\partial U} \bar{D}_0 \bar{v} - \bar{X}_1 \frac{\partial^2 \bar{v}}{\partial U^2} + \frac{\partial \tilde{c}^2}{\partial U} D_0 \tilde{G}_4 + \left[ (\gamma - 1) + \frac{\partial^2 \tilde{c}^2}{\partial U^2} \right] \bar{X}_1 \tilde{G}_4 = 0 \quad (5.30)$$

when  $\tilde{c}^2 = f(U)$  where  $f$  is, at this point, an arbitrary function. Equation(5.26) shows that this reduces to the very simple result

$$\tilde{c}^2 \frac{\partial}{\partial U} \left( \frac{1}{\tilde{c}^2} \bar{D}_0 \bar{v} \right) + \tilde{X}_1 \frac{\partial^2 \bar{v}}{\partial U^2} = 0 \quad (5.31)$$

that only depends on the specific mean flow field through the streamwise component

$$\tilde{X}_1(U, Y) = \bar{X}_1(r(U, Y), Y) \quad (5.32)$$

of the advection vector when  $\tilde{c}^2$  is assumed to satisfy the Crocco relation (Crocco,1932)

$$\tilde{c}^2 = c_\infty^2 - \frac{(\gamma - 1)}{2} U^2 \quad (5.33)$$

Equation (5.32), which is a consequence of the implicit function theorem, merely indicates that  $\bar{X}_1(r, Y)$  becomes a function of  $U, Y$  when  $r$  is expressed as a function of  $U, Y$ . Since equation (A.5) shows that

$$V_r \rightarrow \frac{\tilde{E}(Y)}{2r} \quad \text{as } r \rightarrow \infty \quad (5.34)$$

where

$$\tilde{E}(Y) \equiv \frac{-\tilde{c}^2}{2} \left[ \frac{\partial U_c}{\partial Y} \frac{U_c}{\tilde{c}^2} \left( h + \frac{b}{\sqrt{\ln 2}} \right)^2 - h^2 \frac{d U_c}{d Y} \frac{U_c}{\tilde{c}^2} \right] \quad (5.35)$$

it follows from equations (5.15), (A.1), (A.2) and (A.4) that

$$\tilde{X}_1(U, Y) \rightarrow E(Y)U \quad \text{as } U \rightarrow 0 \quad (5.36)$$

where

$$E(Y) \equiv -\frac{-\tilde{c}^2 U_c \ln 2}{\tilde{c}^2 b^2} \tilde{E}(Y) \quad (5.37)$$

and  $(b, h)$  are parameters that appear in the mean flow model described in appendix A. It therefore follows from (5.21), (5.31) and (5.33) that  $\bar{v}$  satisfies

$$\frac{\partial}{\partial U} \left[ (i\Omega - E(Y))\bar{v} + U \left( E(Y) \frac{\partial \bar{v}}{\partial U} + \frac{\partial \bar{v}}{\partial Y} \right) \right] = 0 \quad (5.38)$$

as  $U \rightarrow 0$ , which means that

$$U \left( E \frac{\partial \bar{v}}{\partial U} + \frac{\partial \bar{v}}{\partial Y} \right) + E \bar{v} = H(Y) \quad (5.39)$$

where  $H(Y)$  is an arbitrary function of  $Y$ . So (as can be verified by direct substitution)  $\bar{v}$  possesses the asymptotic solution

$$\bar{v} = V_0(Y) + V_1(Y)U + \Gamma(Y)Ue^{-i\Omega \ln U/G} + O(U^2 \ln U), \quad \text{as } U \rightarrow 0 \quad (5.40)$$

where  $\Gamma(Y)$  is an arbitrary function of  $Y$  and

$$(i\Omega - E)V_0(Y) = H(Y) \quad (5.41)$$

$$i\Omega\bar{V}_1(Y) + V_0'(Y) = 0 \quad (5.42)$$

It follows that  $\bar{v}$  cannot behave like  $\ln r \sim \ln[\ln(1/U)]^{1/2}$  as  $U \rightarrow 0$  and (see equation(6.1)) therefore, as anticipated, cannot match (5.7) unless  $f(Y), \Phi_0(Y, R, \Omega, 0|\theta) = 0$ . It now follows from (4.1), (4.9), (5.4), (5.5) and (5.8) that  $G_1^{(0)}, G_4^{(0)}$  must satisfy the boundary conditions

$$G_4^{(0)} \rightarrow -i\Omega e^{-i\Omega Y \cos\theta/c_\infty}, \quad (5.43)$$

$$i\Omega G_1^{(0)} \rightarrow -c_\infty^2 \frac{\partial G_4^{(0)}}{\partial Y} = i\Omega c_\infty \cos\theta G_4^{(0)} \quad \text{as } r \rightarrow \infty \text{ with } Y \geq 0 \quad (5.44)$$

As expected (5.40)-(5.42) involve two arbitrary functions that can be specified as boundary conditions along the non-characteristic surface  $U = 0$  and, since (5.15),(5.20),(A.1),(A.2)and (A.3) show that  $G_5^{(0)}$  is exponentially small as  $r \rightarrow \infty$ , it follows that

$$\bar{v} \rightarrow -i\Omega c_\infty^2 e^{-i\Omega Y \cos\theta/c_\infty} \quad (5.45)$$

And equations (5.40) and (5.41) show that this boundary condition will be satisfied if we take

$$H(Y) = -i\Omega c_\infty^2 (i\Omega - E) e^{-i\Omega Y \cos\theta/c_\infty} \quad (5.46)$$

Differentiating (5.40) with respect to  $U$  and using (5.42)shows that

$$\frac{\partial \bar{v}}{\partial U} \rightarrow -\frac{V_0'(Y)}{i\Omega} - \frac{i\Omega}{E} \Gamma(Y) e^{-i\Omega \ln U / G} \quad \text{as } U \rightarrow 0 \quad (5.47)$$

It, therefore, follows from (5.45) and(5.27) that

$$\frac{\partial \bar{v}}{\partial U} \rightarrow i\Omega c_\infty \cos\theta e^{-i\Omega Y \cos\theta/c_\infty} \quad \text{with } Y \geq 0 \quad (5.48)$$

and, therefore, that (5.44) will be satisfied if we set the arbitrary function  $\Gamma$  to zero.

Equation (5.31) is hyperbolic (Garabedian, 1964, p.57 and *ff.*) with characteristics

$$\frac{dY}{dU} = \frac{U}{\tilde{X}_1}, \quad (5.49)$$

or, equivalently

$$Y = \text{constnt}, \quad \frac{dU}{dY} = \frac{\tilde{X}_1}{U} \quad (5.50)$$

This means that it is not necessary to impose a downstream boundary condition, which greatly simplifies the computation. Figure 1 shows the characteristic directions in the  $(Y, U)$  plane (obtained using the difference equation  $U_j = U_{j-1} + (\tilde{X}_{1,j-1}/U_{j-1})(Y_j - Y_{j-1})$  with  $j$  being the grid index along the  $Y$  coordinate) for a subsonic and a supersonic Mach number. Both results suggest that information propagates to the left and to the right from the  $U = 0$  boundary and that no boundary conditions are required on the  $Y = 0$  and  $Y \rightarrow \infty$  boundaries.

The solution is now uniquely determined by the two boundary conditions (5.45) and (5.48) (Garabedian, 1964, p.105) on the non-characteristic curve  $U = 0$ .

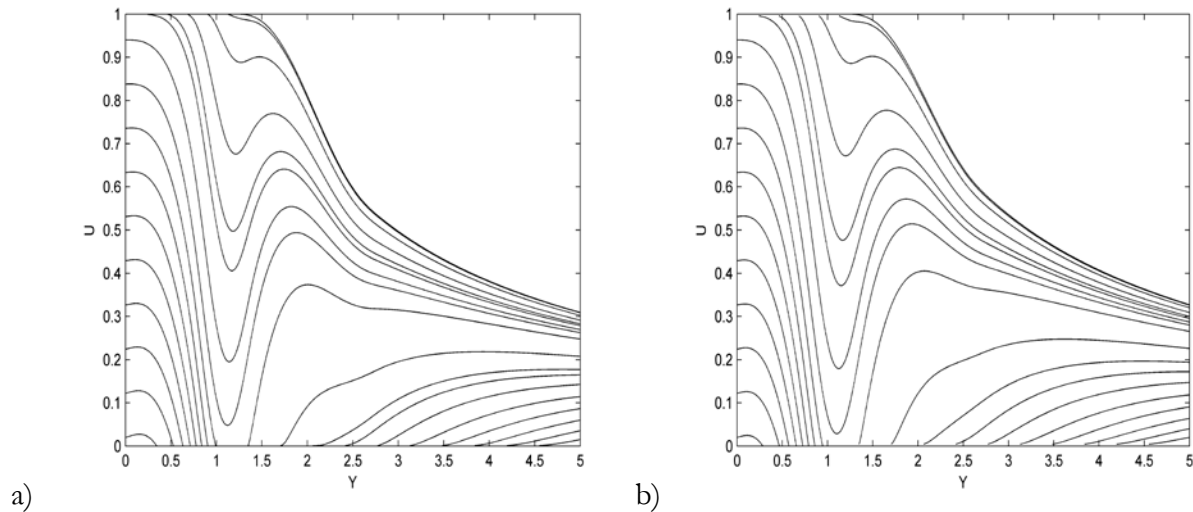


Figure 1 Second family of characteristic curves a) for  $M_\infty = 0.5$  b) for  $M_\infty = 1.4$

$\tilde{G}_4$  can be determined by solving equation (5.26) subject to the initial condition

$$G_4^{(0)} = -i\Omega e^{-i\Omega Y \cos\theta/c_\infty} \quad \text{on } U = 0, \quad \text{with } Y \geq 0 \quad \text{and } \tilde{G}_1 \text{ can then be calculate from (5.23). This}$$

is most easily done by introducing the characteristic coordinates  $\xi(U, Y)$  and  $Y$  where

$\xi = \text{constant}$  is the 2<sup>nd</sup> characteristic curve of (5.31). Then  $\xi$  is an integral of (5.50) and satisfies the partial differential equation (Garabedian, 1964, p.57 and ff.)

$$U \frac{\partial \xi}{\partial Y} + \tilde{X}_1 \frac{\partial \xi}{\partial U} = 0 \quad (5.51)$$

So (5.21) becomes

$$D_0 = i\Omega + U \left( \frac{\partial}{\partial Y} \right)_\xi \quad (5.52)$$

and equation (5.26) can be written as

$$D_0 \left( \tilde{G}_4 - \bar{v} / c^2 \right) = -\bar{X}_1 \frac{\partial}{\partial U} \left( \bar{v} / c^2 \right) \quad (5.53)$$

It, then, follows from equation (5.51) that

$$D_0 \left( \tilde{G}_4 - \bar{v} / c^2 \right) = U \left[ \frac{\partial}{\partial \xi} \left( \bar{v} / c^2 \right) \right] \frac{\partial \xi}{\partial Y} \quad (5.54)$$

which can be integrated along the characteristic  $\xi = \text{constant}$  to obtain

$$\tilde{G}_4(U(\xi, Y), Y) = \tilde{\Gamma}(\xi, Y) + \int_{Y_0}^Y \left[ \exp i\Omega \int_{\hat{Y}}^{\tilde{Y}} \frac{d\hat{Y}}{U(\xi, \hat{Y})} \right] \frac{\partial \tilde{\Gamma}(\xi, \tilde{Y})}{\partial \xi} \tilde{\Lambda}(\xi, \tilde{Y}) d\tilde{Y} \quad (5.55)$$

where

$$\Gamma(U, Y) \equiv \bar{v} / c^2, \quad \tilde{\Gamma}(\xi, Y) \equiv \Gamma(U(\xi, Y), Y), \quad \Lambda(U, Y) \equiv \partial \xi(U, Y) / \partial Y, \quad (5.56)$$

$$\tilde{\Lambda}(\xi, \tilde{Y}) \equiv \Lambda(U(\xi, Y), Y)$$

and  $Y_0$ , which is defined by

$$\xi(0, Y_0) = \xi, \quad (5.57)$$

is the streamwise coordinate of the point where the  $\xi = \text{constant}$  characteristic crosses the non-characteristic line  $U = 0$ .

## 6. Numerical Procedure

Since the general solution to equation (5.31) behaves like (5.40) as  $U \rightarrow 0$ , the derivative  $\partial \bar{v} / \partial U$  will undergo rapid oscillation in the vicinity of  $U = 0$  unless the second term is completely eliminated by the 2<sup>nd</sup> boundary condition(5.48). The numerical procedure, therefore, has to be quite accurate in this region.

Equation (5.31) was solved numerically by rewriting it as a set of two 1<sup>st</sup> order partial differential equations and mapping the  $(Y, U)$  domain into the rectangular  $(\eta, Y)$  domain where  $\eta \equiv U / U_c$ .

The derivatives were approximated with second order finite difference schemes. And since the focus of this paper is on the analytical results, we decided to employ a simple and robust numerical scheme to carry out the computations and use a large number of grid points along with grid convergence studies to make sure that the dissipative character of the scheme did not affect the accuracy of the solution. We were able to use a Lax-Friedrichs scheme (Hirsch, 2001) to solve the resulting set of equations by marching in a pseudo-time direction, since there are no preferential directions along the characteristics (see figure 1). The  $L^2$ -error was used to check the convergence of both  $\bar{v}$  and  $\partial\bar{v}/\partial U$  and the solution was considered to be converged when the error was reduced by approximately 5 orders of magnitude. Figure 2 shows a typical plot of convergence history for  $M_\infty = 0.5$ . Optimizations of the numerical algorithm can certainly be developed by employing one of the high-accurate, non-dissipative schemes that appear in literature.

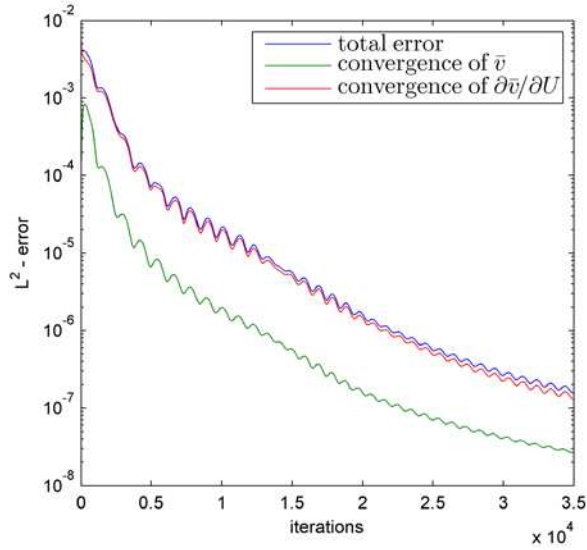


Figure 2. Convergence history for  $M_\infty = 0.5$

$\tilde{G}_1$  was calculated from (5.27) and  $\tilde{G}_4$  was calculated by solving equation (5.26) numerically instead of from the analytical formula (5.55). The results were mapped into the original radial coordinate system by using the equation

$$r(\eta, Y) \rightarrow h + b \sqrt{\frac{\ln \left[ \tilde{c}^2 / \eta \tilde{c}_c^2(Y) \right]}{\ln 2}} \quad (6.1)$$

## 7. Results and Discussion

All computations are based on the compressible mean flow model given in Appendix A and the shear layer parameters  $b(Y)$ ,  $h(Y)$  and  $U_c$  shown in figures A-1, A-2 and A-3, which together

satisfy the momentum conservation relation (A.9). The shear layer inner boundary  $h$  is set equal to 1 at  $Y=0$  since all lengths are normalized by the jet radius  $r_j$  and the centerline velocity  $U_c$  is assumed to be constant in the potential core region. The thickness parameter  $b(Y)$  is assumed to have a constant slope which is adjusted to make the  $h$  value computed from (A.9) go to zero when  $Y = \varepsilon y_1$  is close to 1, since  $r_j$  divided by the potential core length is a reasonable measure of the jet spread rate  $\varepsilon$ . The jet centerline velocity  $U_c$  shown in figure A-3 is computed from (A.11) in the downstream region where  $h = 0$ .

The resulting mean velocity profiles for  $M_\infty = 0.9$  are shown in figure 3. They are nearly identical to the  $M_\infty = 0.5$  and  $M_\infty = 1.4$  results (not shown here).

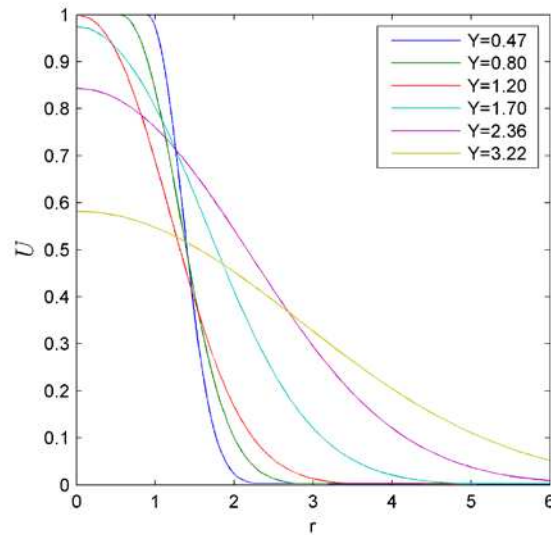


Figure 3 mean velocity profiles for  $M_\infty = 0.9$

Since the boundary conditions (5.45) and the equation obtained by equating the first term in (5.31) to zero are identically satisfied by the locally parallel flow solution

$$\bar{v} = \frac{-i\Omega \tilde{c}^2}{1 - (U/c_\infty)\cos\theta} e^{-i\Omega Y \cos\theta/c_\infty} \quad (7.1)$$

the second term in (5.31) must account for the nonparallel flow effects. Introducing the scaled streamwise coordinate  $\bar{Y} \equiv \Omega Y$  into (5.31) shows that the first term is proportional to  $\Omega$  and therefore becomes dominant as  $\Omega$  becomes large, which confirms that the solution reduces to the locally parallel flow result when the scaled frequency becomes large. Inserting (7.1) into (5.26) and using the result in (5.27) shows that

$$G_1^{(0)} = \frac{-i\Omega \tilde{c}^2 \cos \theta e^{-i\Omega Y \cos \theta / c_\infty}}{c_\infty [1 - (U / c_\infty) \cos \theta]^2} \quad (7.2)$$

when the mean flow is parallel. These results show that  $G_1^{(0)}$  and therefore  $\partial G_1^{(0)} / \partial r$  (which, as noted below makes the dominant contribution to the propagator(2.5)) are identically zero at  $\theta = 90^\circ$  when the mean flow is parallel. We, therefore, expect  $G_1^{(0)}$  and  $\partial G_1^{(0)} / \partial r$  to be small at  $\theta = 90^\circ$  in the non-parallel case. The non-axisymmetric  $n = 1$  contribution to the adjoint Green's function expansion (5.5) and (5.6) should, therefore, be dominant at this angle. But Goldstein (1975, 1976) shows that the  $n = 0$  contribution becomes dominant at small angles when the mean flow is parallel and the Mach number is reasonably large. We expect this to be true in the nonparallel case as well.

Since Karabosov *et al* (2011) show that the nonparallel mean flow effects are insignificant at  $90^\circ$  but can be as large 8 Decibels at  $30^\circ$  to the downstream axis, we focus on the small angle radiation where the axisymmetric contribution to the low frequency Green's function is dominant. It is , therefore, only necessary to consider the  $n = 0$  contribution to the expansion (5.5) and (5.6) which is determined by the very simple hyperbolic equation (5.31). Its solution is, as noted in section 5, only affected by the mean flow through streamwise component  $\tilde{X}_1$  of the mean flow advection vector.

This quantity is plotted in figure 4 for  $M_\infty = 0.5$  and  $M_\infty = 1.4$ . Notice that the results are nearly identical. The curves in parts a) and b) start from the edge of the potential core when  $Y < 1$  and from the jet centerline,  $r = 0$ , when  $Y > 1$ . The curves in parts c) and d) of the figure show that  $\tilde{X}_1$  changes very rapidly in the zone between the end of the potential core and the transition region. The effective spread rate is, therefore, expected to be very large when the source point is located in this region, which suggests the non-parallel effects will continue to be important at larger values of the Strouhal number. But this could also cause the asymptotic solution to break down at relatively small values of the expansion parameter  $\varepsilon$ , which means that the full numerical solution would have to be invoked for relatively small values of this parameter.

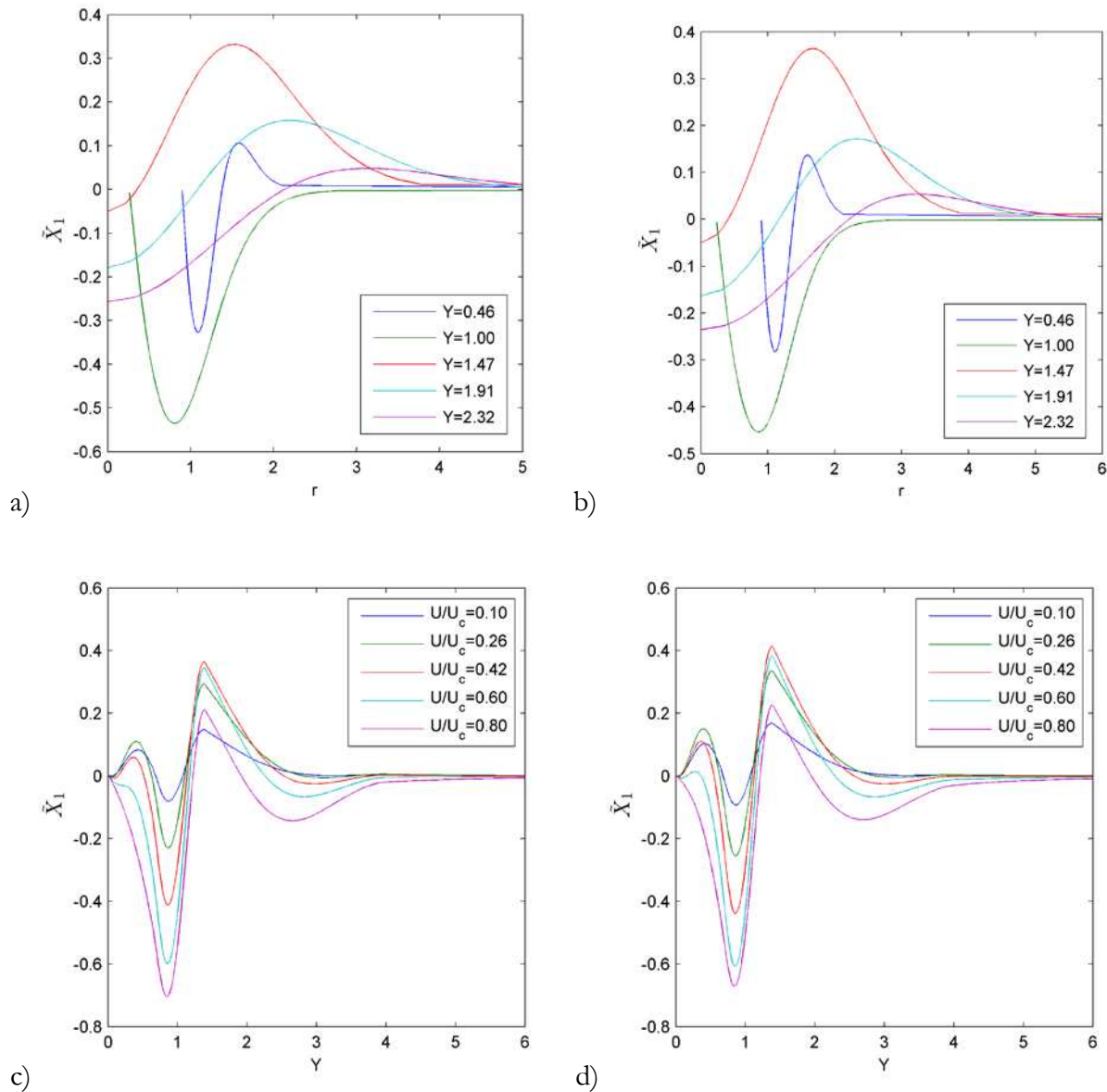


Figure 4. Streamwise component of the mean flow advection vector profiles a) as a function of  $r$  for fixed  $Y$  and  $M_\infty = 0.5$ , b) as a function of  $r$  for fixed  $Y$  and  $M_\infty = 1.4$  c) as a function of  $Y$  for fixed  $U/U_c$  and  $M_\infty = 0.5$ , d) as a function of  $Y$  for fixed  $U/U_c$  and  $M_\infty = 1.4$

Figures 5-7 are plots of the intermediate variable  $\bar{v}$  calculated from (5.31) and (5.45) as a function of the mean streamwise velocity  $U$  at various values of the streamwise coordinate  $Y$  for three different Mach numbers. These plots show that this quantity is fairly close to the corresponding parallel flow solution at low Mach numbers and that, as expected, it converges to that solution as  $\Omega$  increases. But they also show that the convergence occurs at progressively higher frequencies as the Mach number increases and that the supersonic result never converges to this result in the vicinity of the critical layer (which lies at  $U = 0.8247$  in the figure) where the denominator of (7.1) vanishes.

This is because the parallel flow solution has a singularity at the critical layer and, therefore, becomes invalid in that region for any finite value of  $\Omega$ . This occurs because the non-parallel flow effects will always be important in a sufficiently small region surrounding the critical layer no matter how small the mean flow divergence rate  $\varepsilon$  becomes.

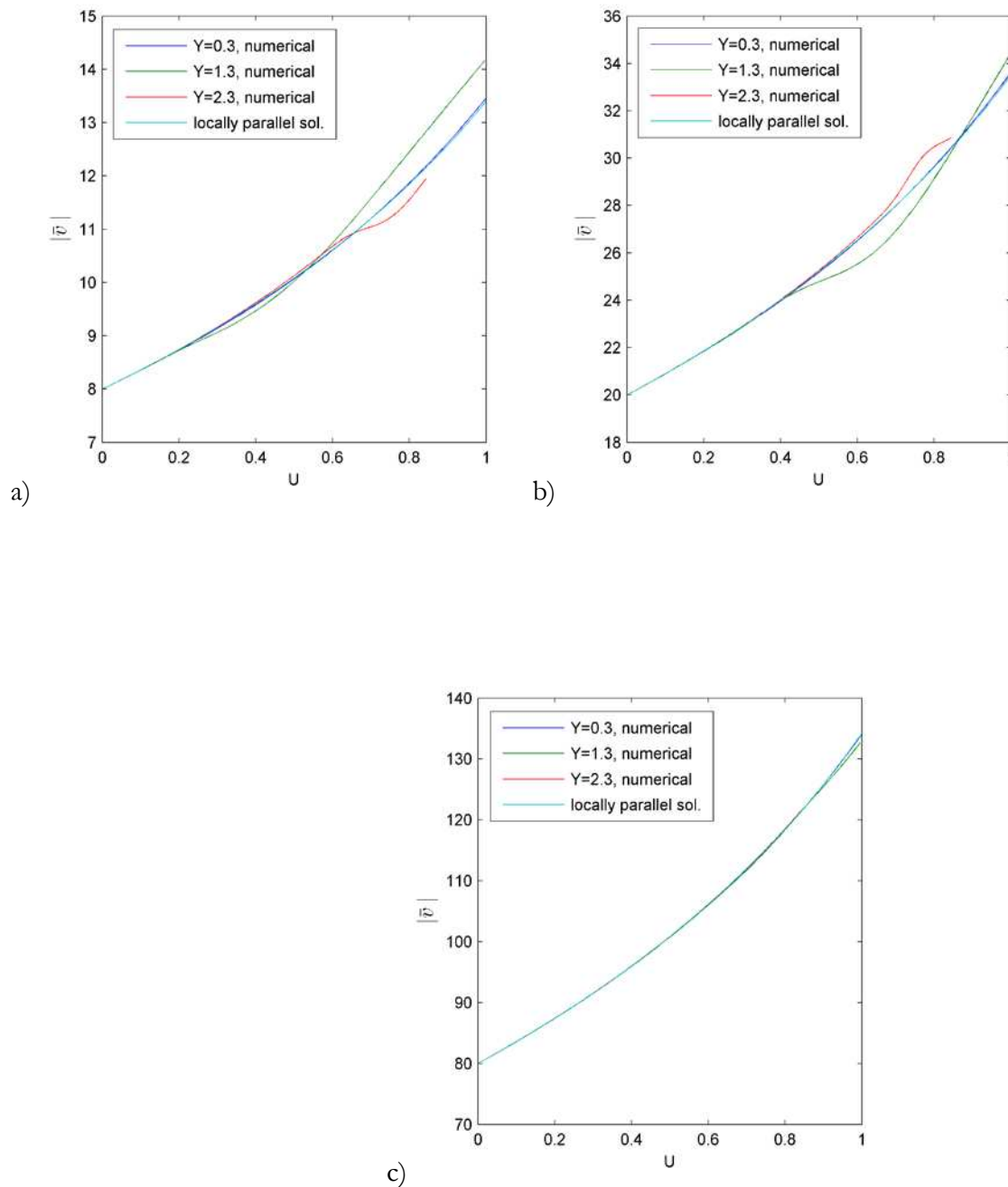


Figure 5. Plots of intermediate dependent variable  $|\bar{v}|$  vs.  $U$  at constant  $Y$  for  $\theta = 30^\circ$ ;  $M_\infty = 0.5$ ;

a)  $\Omega = 2$ ; b)  $\Omega = 5$  c)  $\Omega = 20$

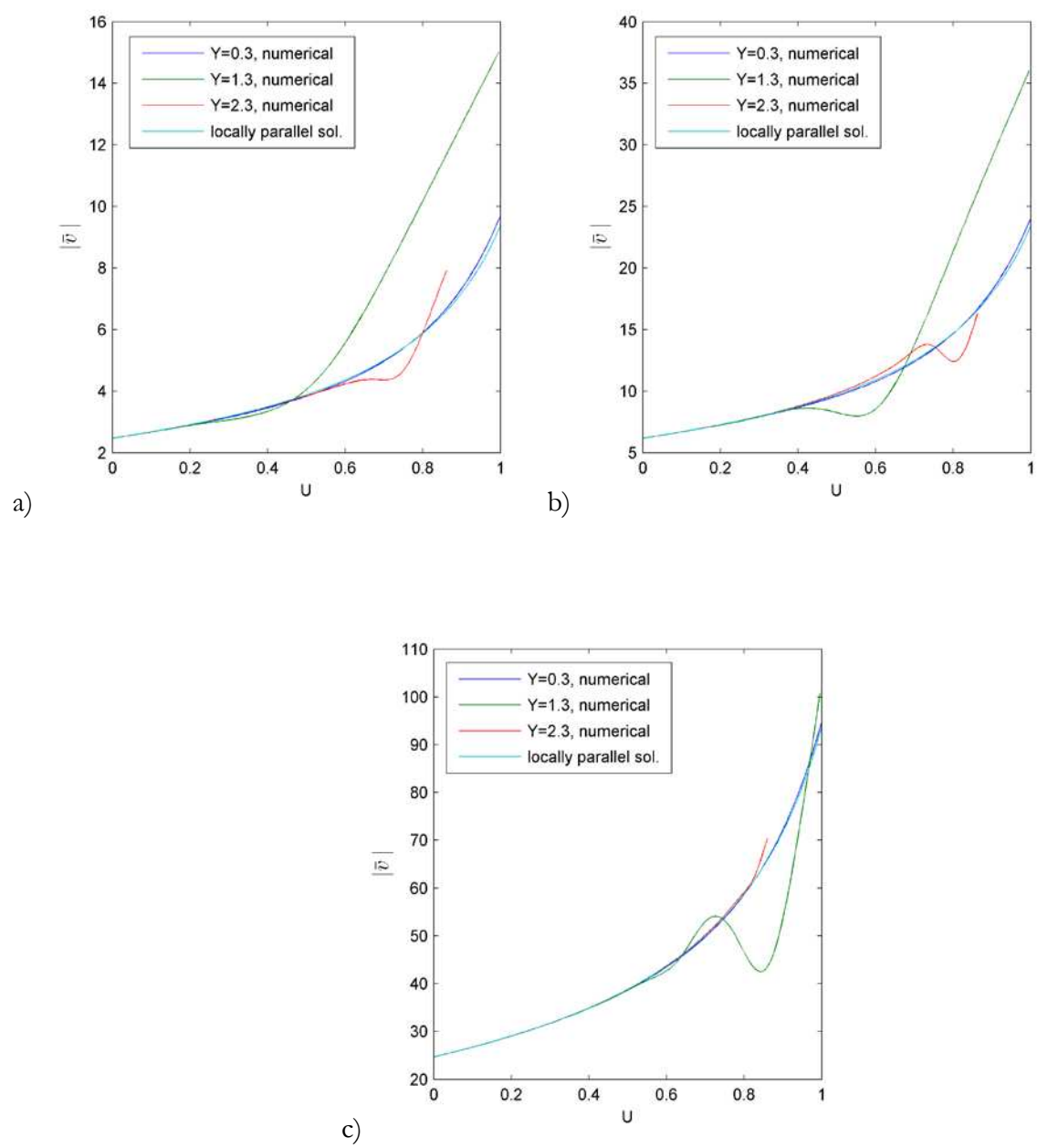


Figure 6. Plots of intermediate dependent variable  $|\bar{v}|$  vs.  $U$  at constant  $Y$  for  $\theta = 30^\circ$ ;  $M_\infty = 0.9$ ; a)  $\Omega = 2$ ; b)  $\Omega = 5$  c)  $\Omega = 20$

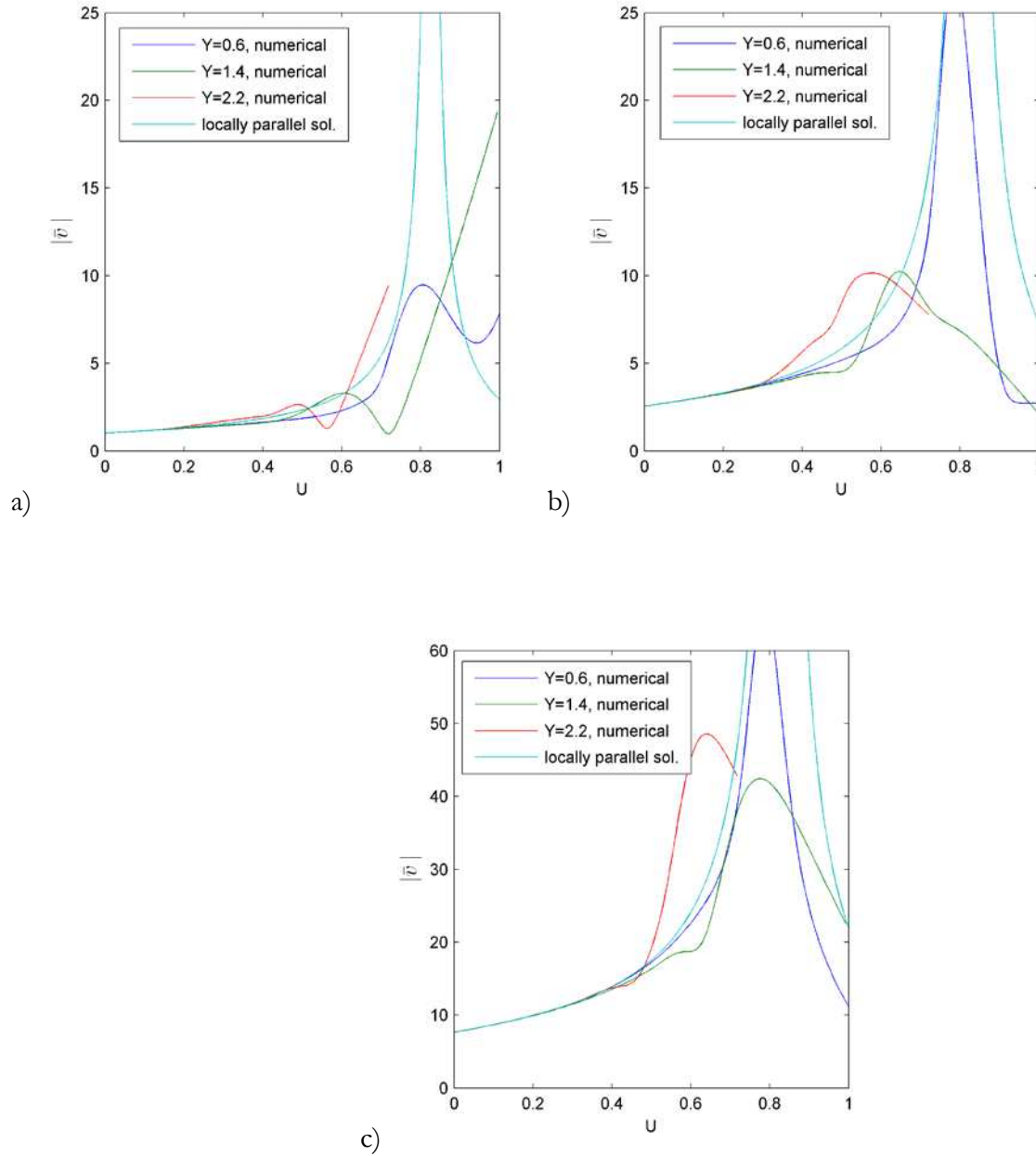


Figure 7. Plots of intermediate dependent variable  $|\bar{v}|$  vs.  $U$  at constant  $Y$  for  $\theta = 30^\circ$ ;  $M_\infty = 1.4$ ;  
a)  $\Omega = 2$ ; b)  $\Omega = 5$  c)  $\Omega = 15$

It follows from equations (2.4) and (2.5) that the largest contribution to the far field spectra comes from the streamwise  $G_1^{(0)}$  component of the Fourier transformed Green's function. This quantity can be obtained from equations(5.22) and (5.55) by quadratures but the results shown for three different acoustic Mach numbers in figures 8-10 are obtained from the  $\bar{v}$  solutions by integrating

the first order differential equation (5.26) numerically. The results show that, while  $|G_1^{(0)}|$  again converge to the locally parallel flow result (now given by (7.2)) as  $\Omega$  becomes large, the deviation between these results is now considerably larger and the convergence is much slower than it was for  $|\bar{v}|$ . This is probably because the derivatives that appear in equation (5.23) tend to amplify these differences.

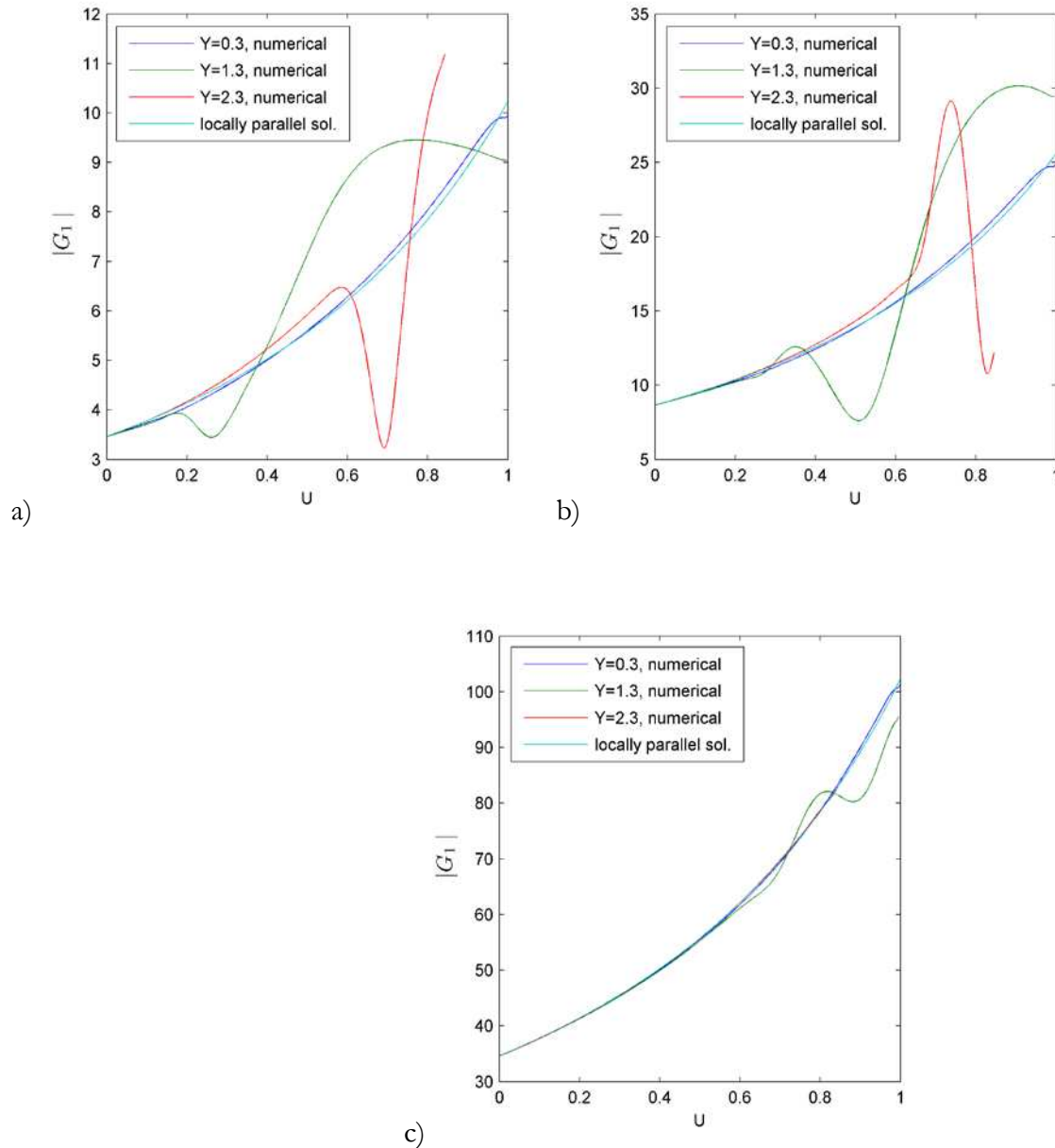


Figure 8. Comparison of parallel and nonparallel solutions for  $|G_1^{(0)}|$  vs.  $U$  at constant  $Y$  for

$\theta = 30^\circ$ ;  $M_\infty = 0.5$ ; a)  $\Omega = 2$ , b)  $\Omega = 5$ , c)  $\Omega = 20$

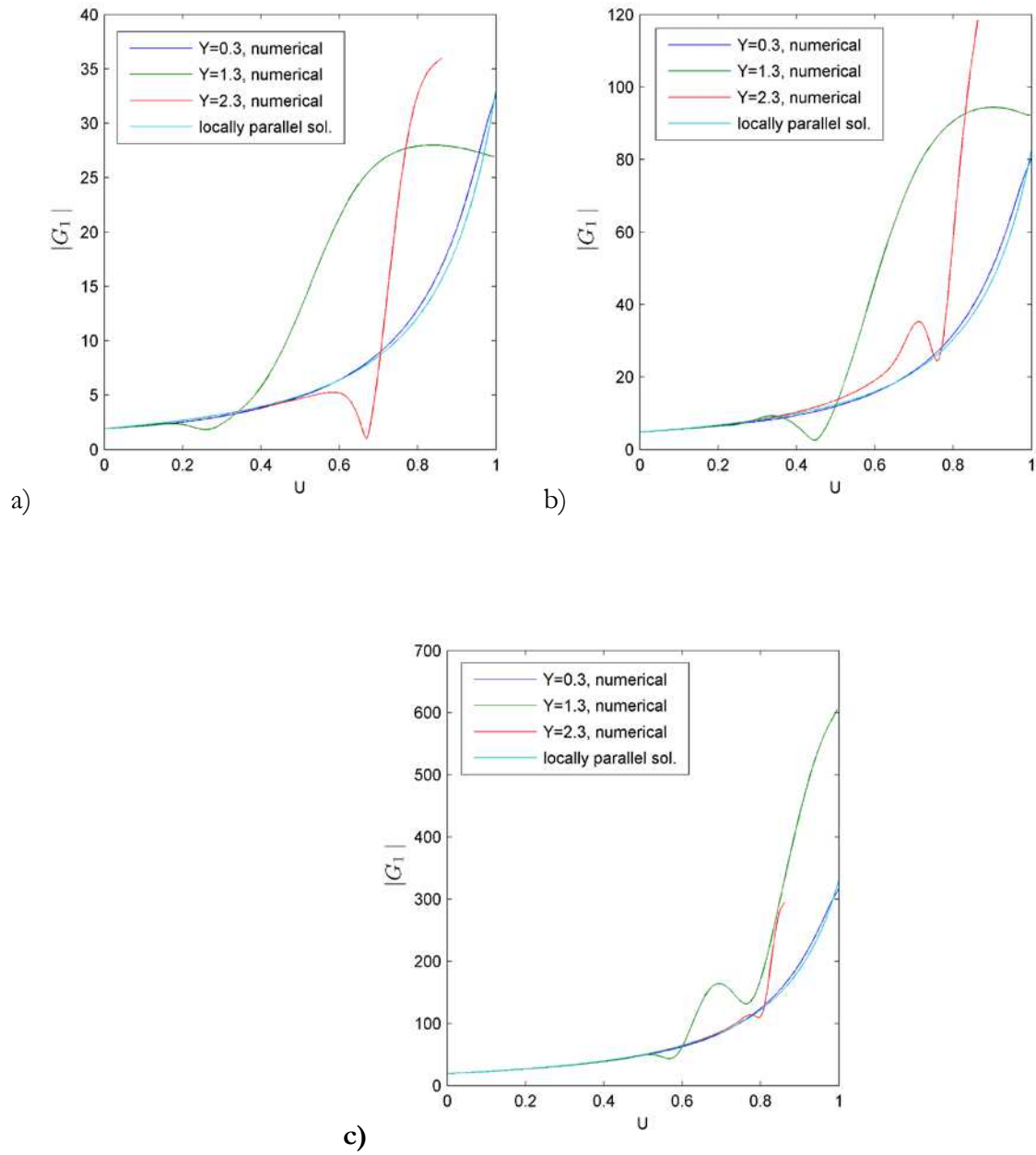


Figure 9. Comparison of parallel and nonparallel solutions for  $|G_1^{(0)}|$  vs.  $U$  at constant  $Y$  for

$\theta = 30^\circ$  ;  $M_\infty = 0.9$ ; a)  $\Omega = 2$ , b)  $\Omega = 5$ , c)  $\Omega = 20$

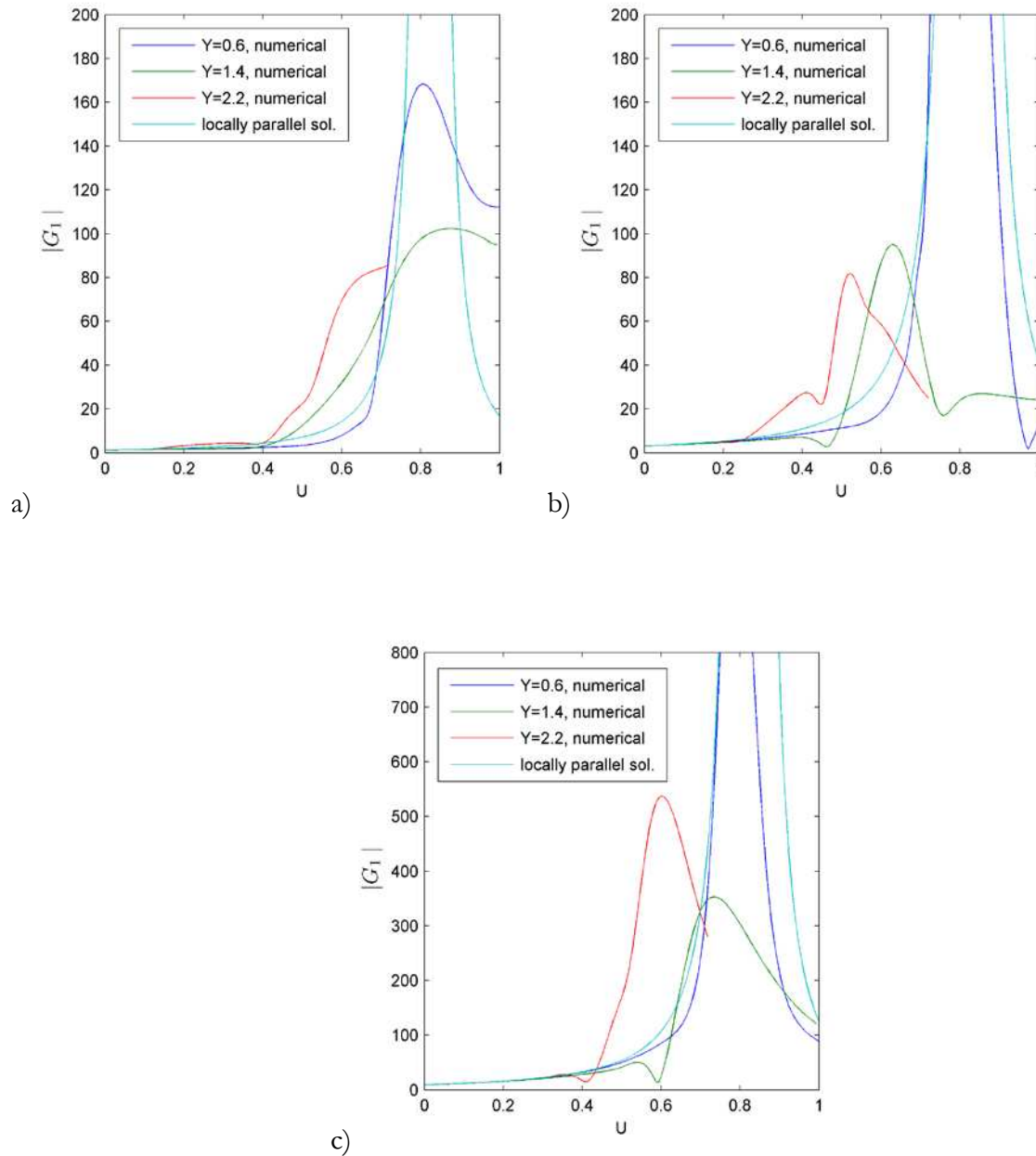


Figure 10. Comparison of parallel and nonparallel solutions for  $|G_1^{(0)}|$  vs.  $U$  at constant  $Y$  for  $\theta = 30^\circ$ ;  $M_\infty = 1.4$ ; a)  $\Omega = 2$ ; b)  $\Omega = 5$  c)  $\Omega = 15$

The dominant contribution to the propagator(2.5) comes from the radial derivative of  $G_1^{(0)}$ . Figures 11-22 show  $|\partial G_1^{(0)} / \partial r|$  for  $M_\infty = 0.5, 0.9, 1.4$ . Since the dependent variable  $y$  corresponds the actual physical source point in the adjoint problem while the source variable  $x$  corresponds to the actual “observation point, these altitude plots represent the intensity of the radiated sound as a function of source location. They show, among other things, that the parallel

flow solutions exhibit a single peak (centered on the initial shear layer at subsonic speeds), while the non-parallel solutions exhibit a double peak structure with the second peak is centered on the nozzle lip line about two potential core lengths downstream. This causes a large increase in the magnitude of  $|\partial G_1^{(0)} / \partial r|$  at subsonic Mach numbers, which decreases with increasing Mach number. The primary nonparallel flow effect at supersonic speeds is to prevent  $|\partial G_1^{(0)} / \partial r|$  from becoming infinite in the critical layer (i.e., to eliminate the critical layer singularity that occurs in the parallel flow solution). These results highlight the importance of non-parallel flow effects in identifying apparent source locations at low frequencies, since they show that the parallel flow Green's function incorrectly predicts the source location by a significant amount--as was first pointed out by Karabasov (2010).

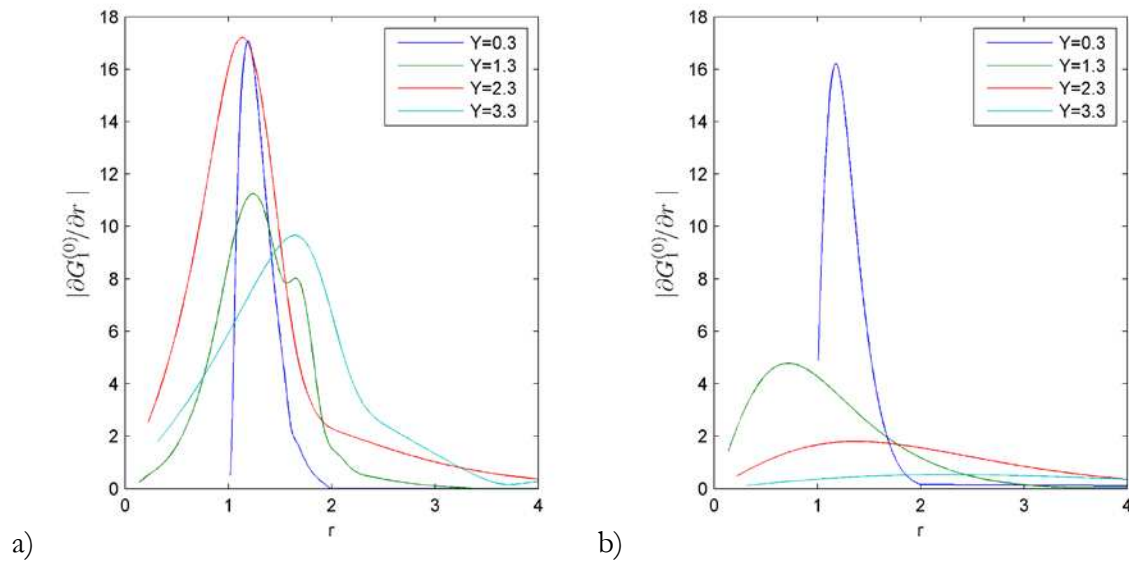
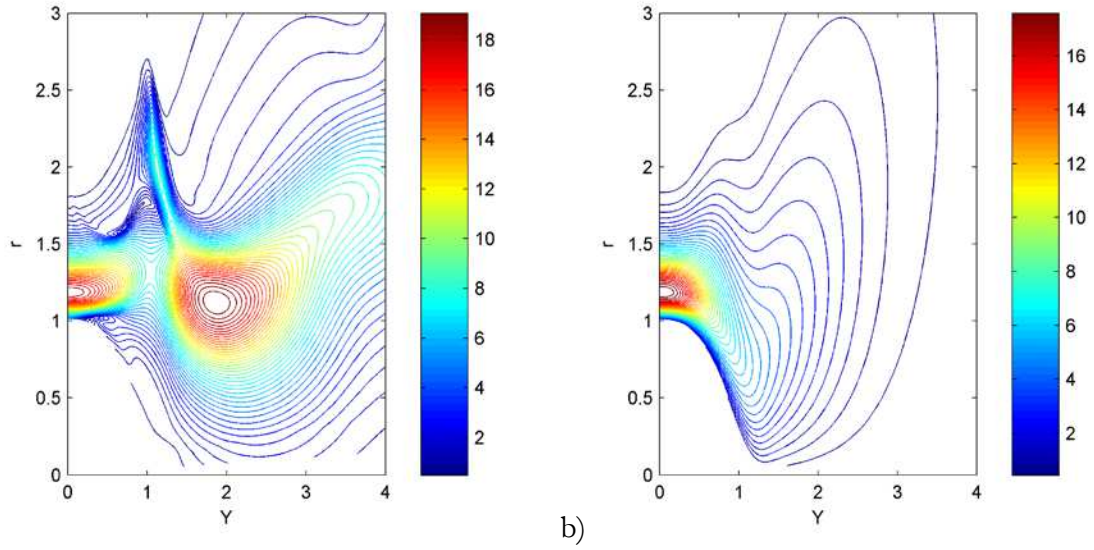
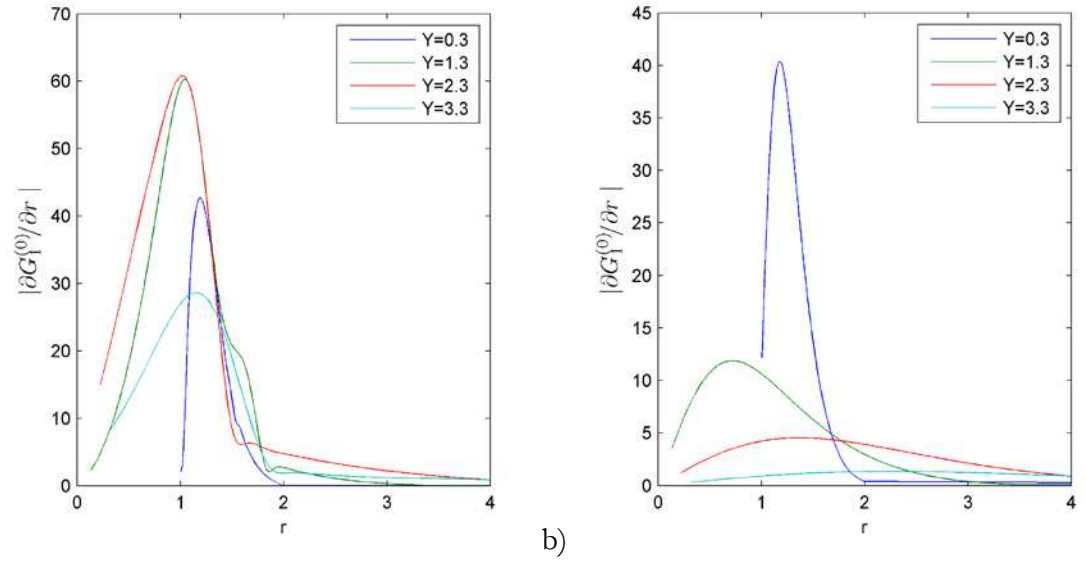


Figure 11. Plots of  $|\partial G_1^{(0)} / \partial r|$  vs.  $r$  at various values of  $Y$  for  $\Omega = 2$ ;  $\theta = 30^\circ$ ;  $M_\infty = 0.5$ ; a) nonparallel, b) parallel mean flow



a) b)  
 Figure 12. Contour plots of  $\left| \frac{\partial G_1^{(0)}}{\partial r} \right|$  for  $\Omega = 2$ ;  $\theta = 30^\circ$ ;  $M_\infty = 0.5$ ; a) nonparallel, b) parallel mean flow



a) b)  
 Figure 13. Plots of  $\left| \frac{\partial G_1^{(0)}}{\partial r} \right|$  vs.  $r$  at various values of  $Y$  for  $\Omega = 5$ ;  $\theta = 30^\circ$ ;  $M_\infty = 0.5$ ; a) nonparallel, b) parallel mean flow

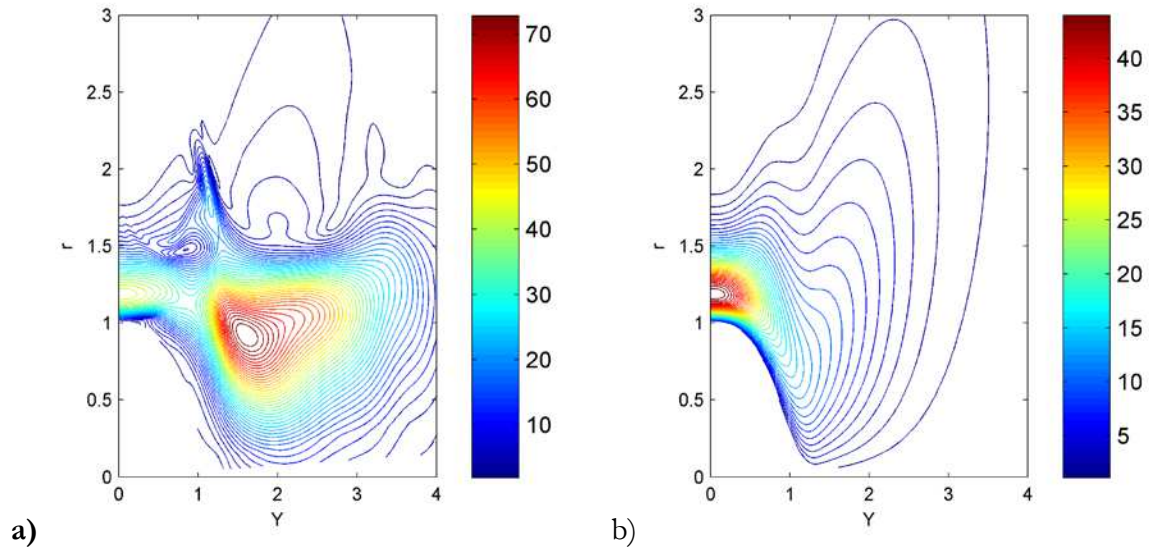


Figure 14. Contour plots of  $\left| \frac{\partial G_1^{(0)}}{\partial r} \right|$  for  $\Omega = 5$ ;  $\theta = 30^\circ$ ;  $M_\infty = 0.5$ ; a) nonparallel, b) parallel mean flow

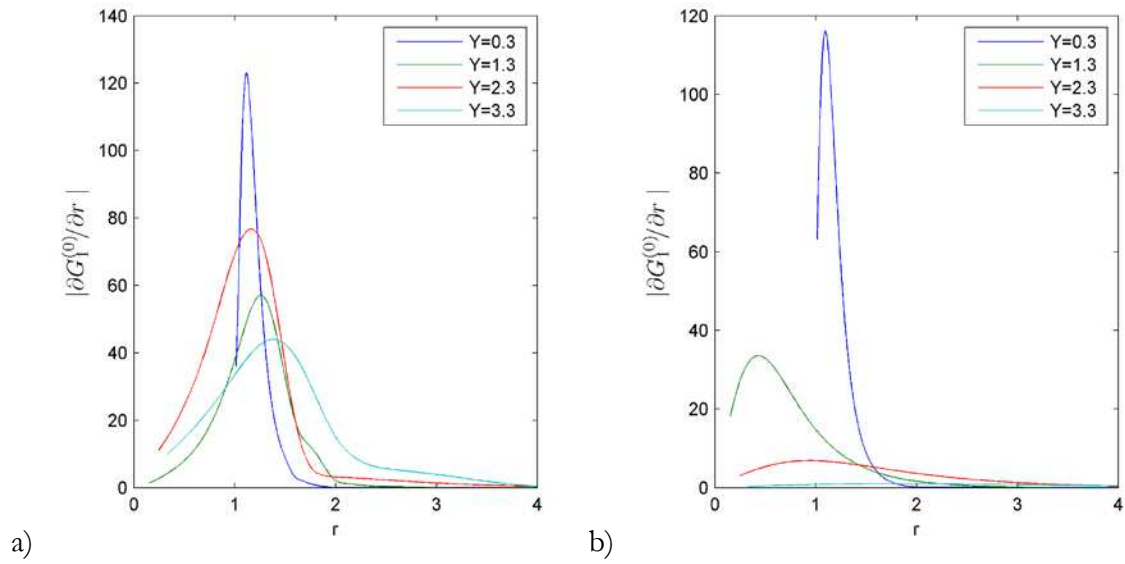


Figure 15. Plots of  $\left| \frac{\partial G_1^{(0)}}{\partial r} \right|$  vs.  $r$  at various values of  $Y$  for  $\Omega = 2$ ;  $\theta = 30^\circ$ ;  $M_\infty = 0.9$ ; a) nonparallel, b) parallel mean flow

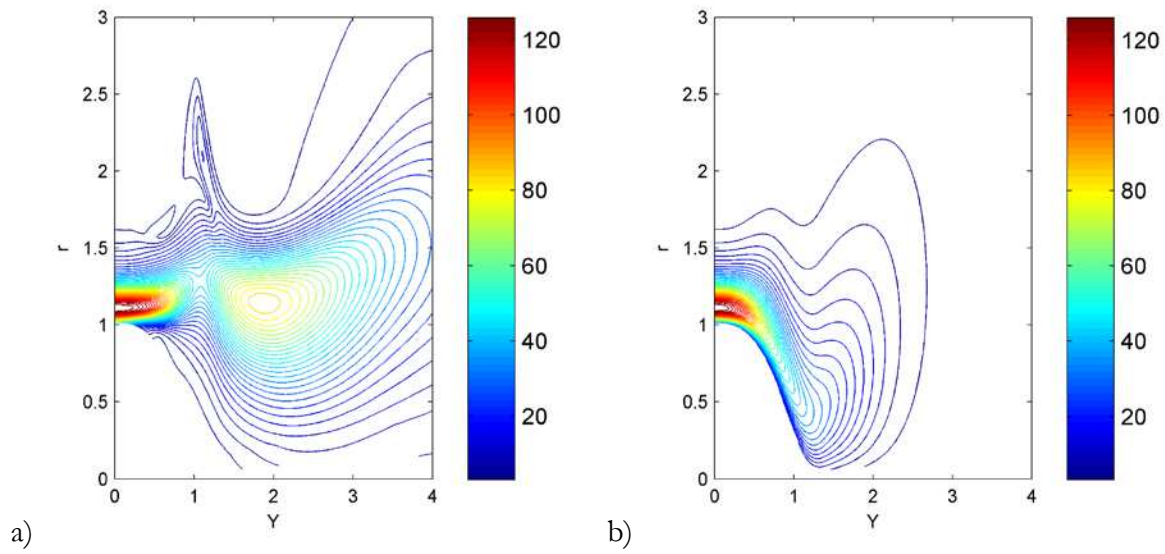


Figure 16. Contour plots of  $|\partial G_1^{(0)} / \partial r|$  for  $\Omega = 2$ ;  $\theta = 30^\circ$ ;  $M_\infty = 0.9$ ; a) nonparallel, b) parallel mean flow

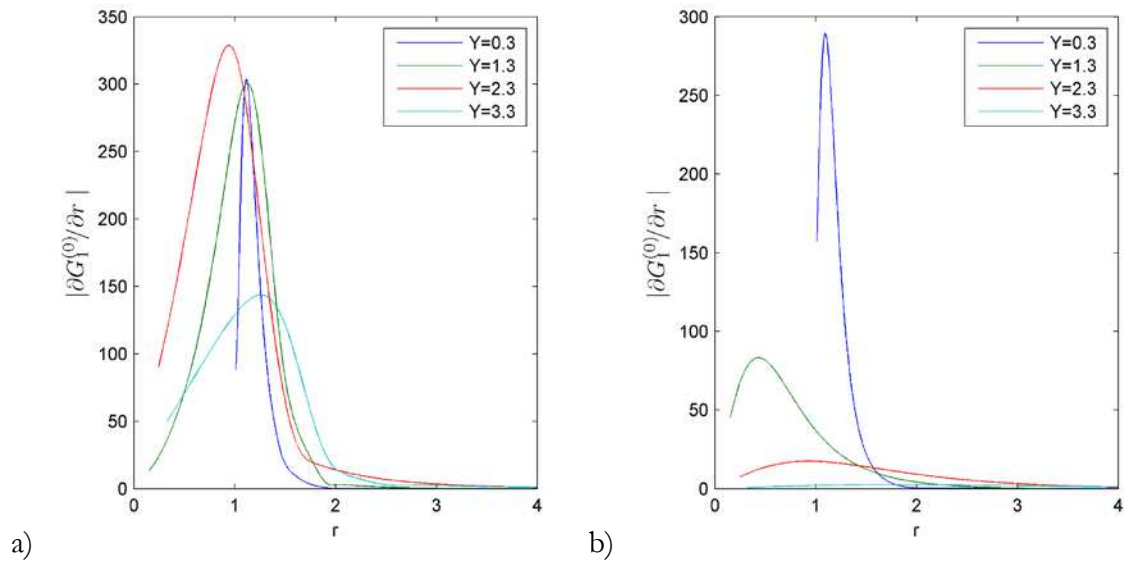


Figure 17. Plots of  $|\partial G_1^{(0)} / \partial r|$  vs.  $r$  at various values of  $Y$  for  $\Omega = 5$ ;  $\theta = 30^\circ$ ;  $M_\infty = 0.9$ ; a) nonparallel, b) parallel mean flow

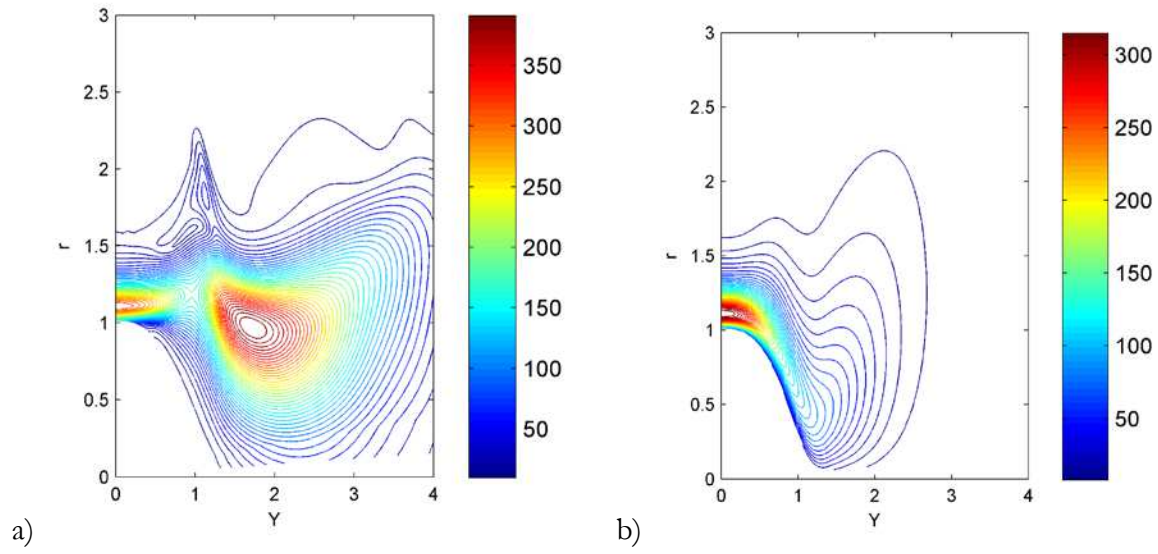


Figure 18. Contour plots of  $\left| \frac{\partial G_1^{(0)}}{\partial r} \right|$  for  $\Omega = 5$ ;  $\theta = 30^\circ$ ;  $M_\infty = 0.9$ ; a) nonparallel, b) parallel mean flow

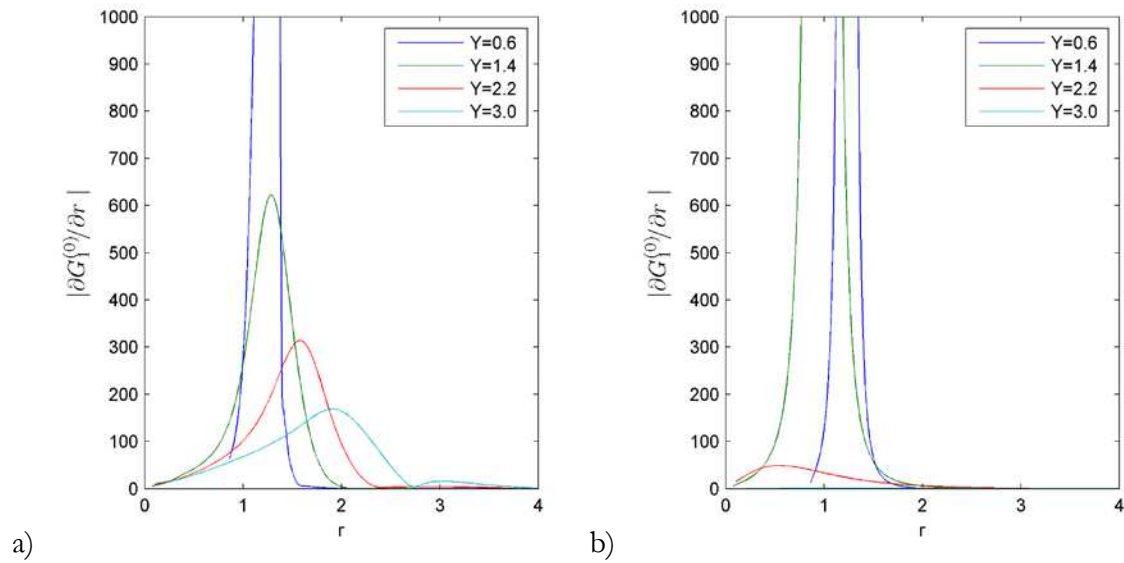


Figure 19. Plots of  $\left| \frac{\partial G_1^{(0)}}{\partial r} \right|$  vs.  $r$  at various values of  $Y$  for  $\Omega = 2$ ;  $\theta = 30^\circ$ ;  $M_\infty = 1.4$ ; a) nonparallel, b) parallel mean flow

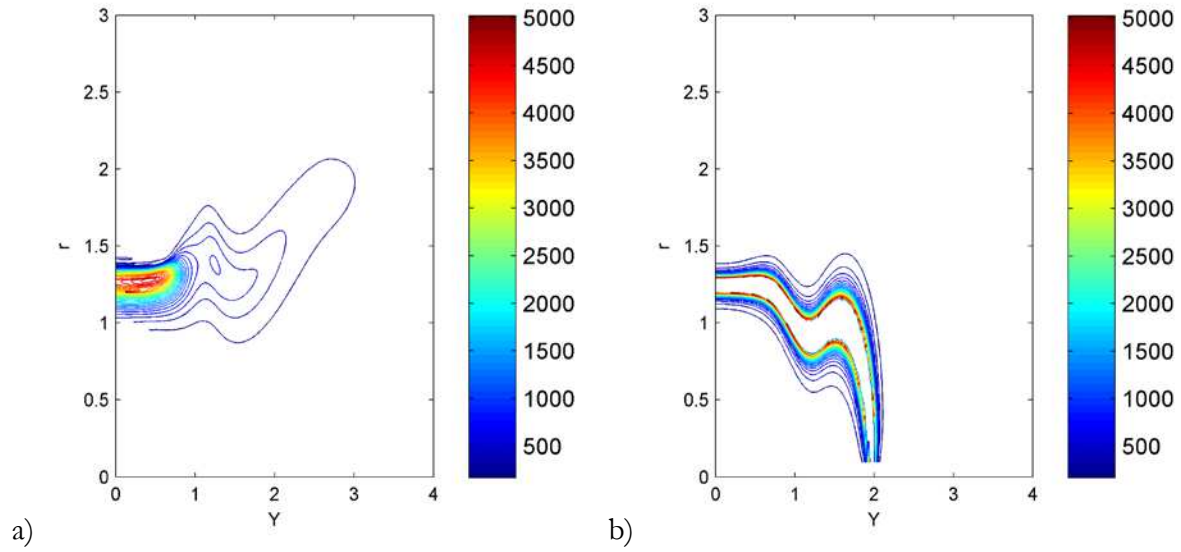


Figure 20. Contour plots of  $|\partial G_1^{(0)} / \partial r|$  for  $\Omega = 2$ ;  $\theta = 30^\circ$ ;  $M_\infty = 1.4$ ; a) nonparallel, b) parallel mean flow

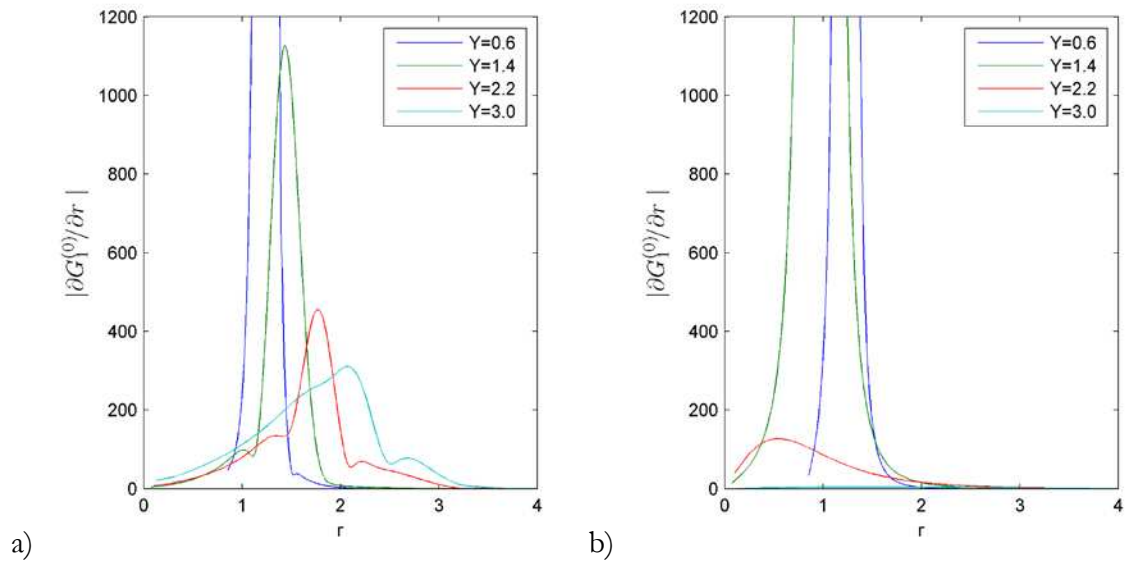


Figure 21. Plots of  $|\partial G_1^{(0)} / \partial r|$  vs.  $r$  at various values of  $Y$  for  $\Omega = 5$ ;  $\theta = 30^\circ$ ;  $M_\infty = 1.4$ ; a) nonparallel, b) parallel mean flow

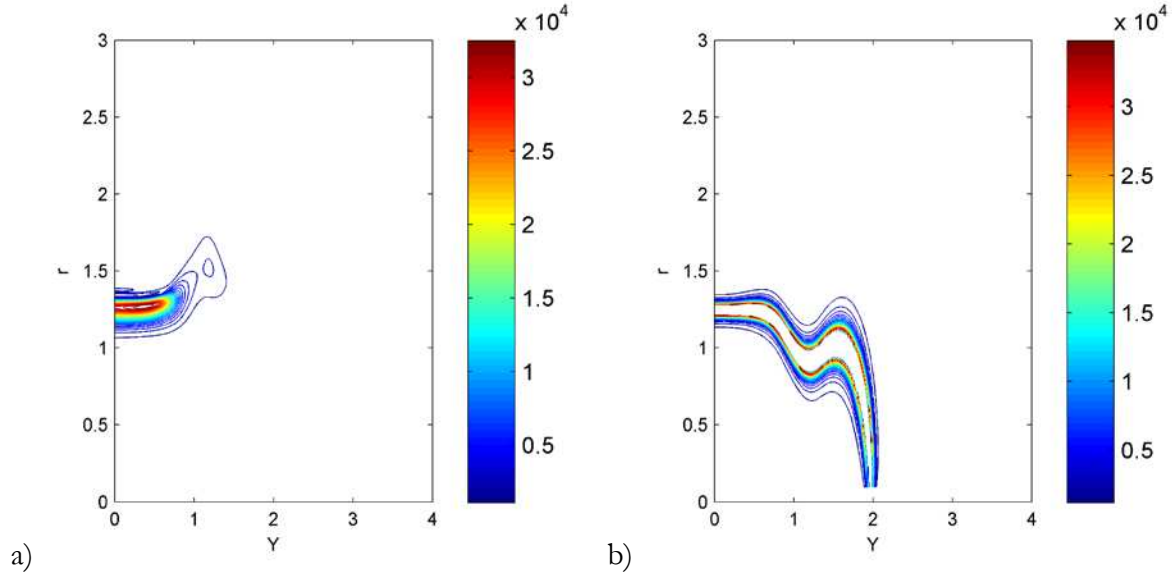
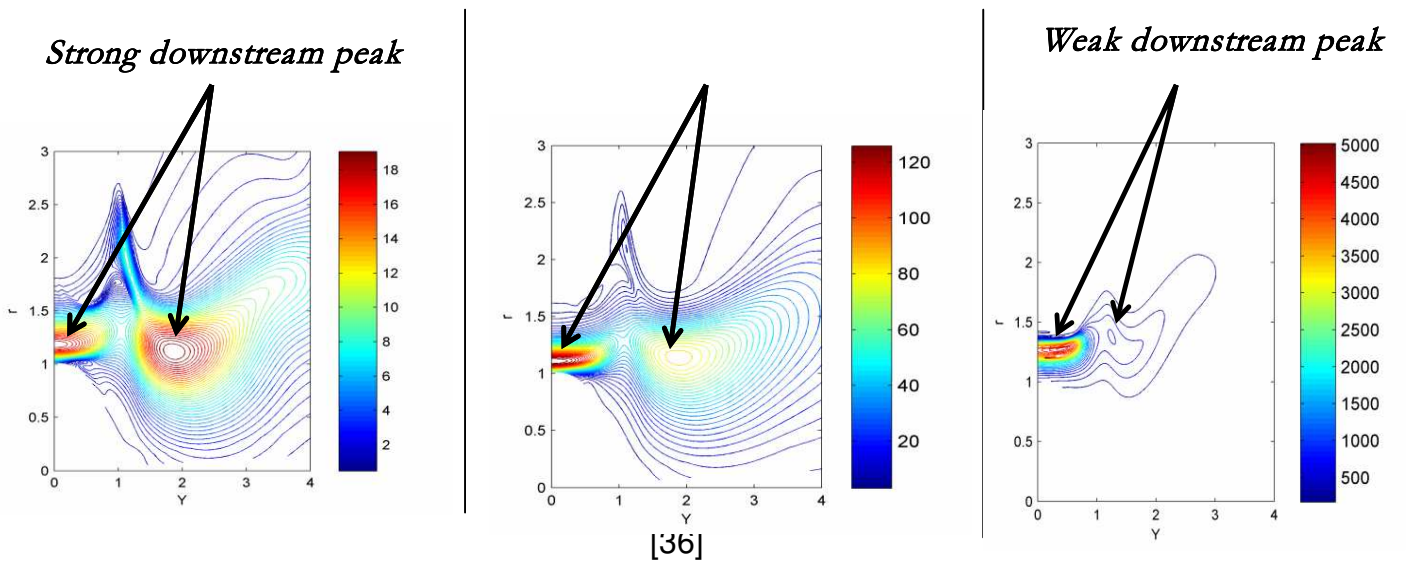


Figure 22. Contour plots of  $\left| \frac{\partial G_1^{(0)}}{\partial r} \right|$  for  $\Omega = 5$ ;  $\theta = 30^\circ$ ;  $M_\infty = 1.4$ ; a) nonparallel, b) parallel mean flow

The downstream peak appears to be associated with the positive peak in the mean flow advection vector  $\tilde{X}_1$  which, as shown in parts c) and d) of figure 4, lies in a region where the mean velocity gradient  $\partial U / \partial r$  is still fairly large. The larger negative values tend to lie in a region where  $\partial U / \partial r$  is small. These effects only occur at small angles to the downstream axis and decrease with increasing  $\Omega$ . The nonparallel effects are completely opposite at supersonic and subsonic speeds. Comparison of parts a) and b) of figures 11-20 shows that the deviations between the parallel and non-parallel flow results are much larger than they were for  $\bar{v}$ . This can probably be attributed to the fact that the  $\partial r / \partial U$  derivative becomes very large in some regions of the flow.

The double peaked structure occurs at all Mach numbers but the upstream peak increases in magnitude and dominates over the downstream peak at supersonic speeds as shown in figure (23).



(24a). M = 0.5

(24b). M = 0.9

(24c). M = 1.4

Figure 23. Change in the “two-peak” structure with Mach number for  $\Omega = 2$ .

Equation (2.4) shows that the actual acoustic spectrum is determined by the product of the Fourier transformed propagator with a large number components of a tensor  $\mathcal{H}_{\lambda j \kappa l}$ ,  $j, l = 1, 2, 3$ :

$\lambda, \kappa = 1, 2, 3, 4$  that characterizes the acoustic source and that a number of these will appear in the formula even when the propagator is approximated by the single  $\partial G_1 / \partial r$  term. But G & L and Afsar (2011) show that only the single  $\mathcal{H}_{1r1r}$  component appears when some plausible assumptions are made about the tensorial structure of the turbulence.

These results are consistent with the Karabasov *et al* (2011) numerical results, which show that nonparallel flow increases the low frequency sound radiated at small angles to the jet axis in a Mach 0.9 jet (their Figure 16(b)) and that the largest effect occurs when the source is about nine diameters (or about two potential core lengths) downstream from the nozzle (see figure 9 of Karabasov et al, 2011). Their results also show that the nonparallel flow does not affect the sound radiated at  $90^\circ$  to the downstream axis at any frequency.

$G_\lambda(\mathbf{y}|\mathbf{x};\omega)$  is the Fourier transform of the 4<sup>th</sup> component  $g_{\lambda 4}^a(\mathbf{y}, \tau|\mathbf{x}, t)$  of the adjoint vector Green's function of a specific form of the linearized Euler equations. These equations can be written in a number of different ways by using the Steady Euler equations to change the way their coefficients depend on the base flow variables. But the only form corresponding to the adjoint equations (2.8)-(2.10) is compatible with the generalized acoustic analogy and, therefore with the acoustic formula(2.4).. Tam and Auriault (1998) use a different form of the adjoint Green's function equation to compute the acoustic radiation from a point source at a particular location in a non-parallel mean flow. Their results shown in their figures 11-13 suggest that the low frequency sound will be relatively insensitive to nonparallel mean flow effects at subsonic Mach numbers. But their computations are based on the 4<sup>th</sup> component  $g_{44}^a$  of the adjoint vector Green's function while the present analysis shows that it is the radial derivative of the  $g_{14}^a$  component that makes the dominant contribution to the propagator (2.5) that appears in the acoustic formula (2.4) and is, therefore, the dominant source of the low frequency sound radiation at small angles to the downstream axis. The calculations displayed in figures 5-7 show that the derived function  $\bar{v}$ , which roughly corresponds to  $g_{44}^a$ , is relatively insensitive to non-parallel flow effects except where critical layer effects come into play in supersonic flows--as predicted by Tam and Auriault (1998). But figures 11-19 show that the  $\partial g_{14}^a / \partial r$  term can be strongly affected by nonparallel mean flow effects for certain source locations that lie in regions where the turbulence intensity is likely to be fairly high--suggesting that the low frequency sound will be strongly affected by nonparallel mean flow effects as found by Karabosov *et al* (2011).

## 8. Concluding Remarks

The far field acoustic spectrum can be expressed as the product of a propagator (that accounts for the mean flow interactions) and a generalized Reynolds stress auto-covariance tensor (that accounts for the turbulent fluctuations). The propagator only depends on the mean flow and the adjoint vector Green's function for a particular form of the linearized Rayleigh equations for that flow. This paper is concerned with the effects of the nonparallel mean flow on the low frequency limit of that Green's function. It is shown that this quantity can be calculated by solving a very simple second order hyperbolic equation of a derived function  $\bar{v}$ . The numerical results show that this quantity is fairly close to the corresponding parallel flow result at low Mach numbers and that, as expected, it converges to this solution as the scaled frequency parameter  $\Omega$  increases. But they also show that the at progressively higher frequencies as the Mach number increases and that the supersonic result never converges to this solution in the vicinity of its critical layer.

The dominant contribution to the propagator (2.5) comes from the radial derivative  $\left| \partial G_1^{(0)} / \partial r \right|$  of streamwise component,  $G_1^{(0)}$ , of the Fourier transform of the adjoint vector Green's function. Altitude plots of  $\left| \partial G_1^{(0)} / \partial r \right|$  as a function of source location  $(r, Y)$  show that while the parallel flow solutions exhibit a single peak centered on the initial shear layer, the non-parallel solutions exhibit a double peak structure with the second peak occurring in a region centered on the nozzle lip line about two potential core lengths downstream. This causes a large increase in the magnitude of  $\left| \partial G_1^{(0)} / \partial r \right|$  at subsonic Mach numbers, which decreases with increasing Mach number. The primary nonparallel flow effect at supersonic speeds is to prevent  $\left| \partial G_1^{(0)} / \partial r \right|$  from becoming infinite in the critical layer (i.e., to eliminate the critical layer singularity that occurs in the parallel flow solution). The nonparallel effects, therefore, produce completely opposite changes in  $\left| \partial G_1^{(0)} / \partial r \right|$  at supersonic and subsonic speeds. The figures show that the deviations between the parallel and non-parallel flow results for  $\left| \partial G_1^{(0)} / \partial r \right|$  are now much larger than they are for  $\bar{v}$ . These results appear to be consistent with the Karabasov *et al* (2011) numerical computations, which show that the nonparallel flow increases the low frequency sound radiated at small angles to the jet axis in a Mach 0.9 jet (their Figure 16(b)). Figure (9b) of this reference shows that the largest non-parallel flow effects occur when the source is located about two potential core lengths downstream of the nozzle. Figure 24 shows the qualitative similarity of this figure with our figure (18a).

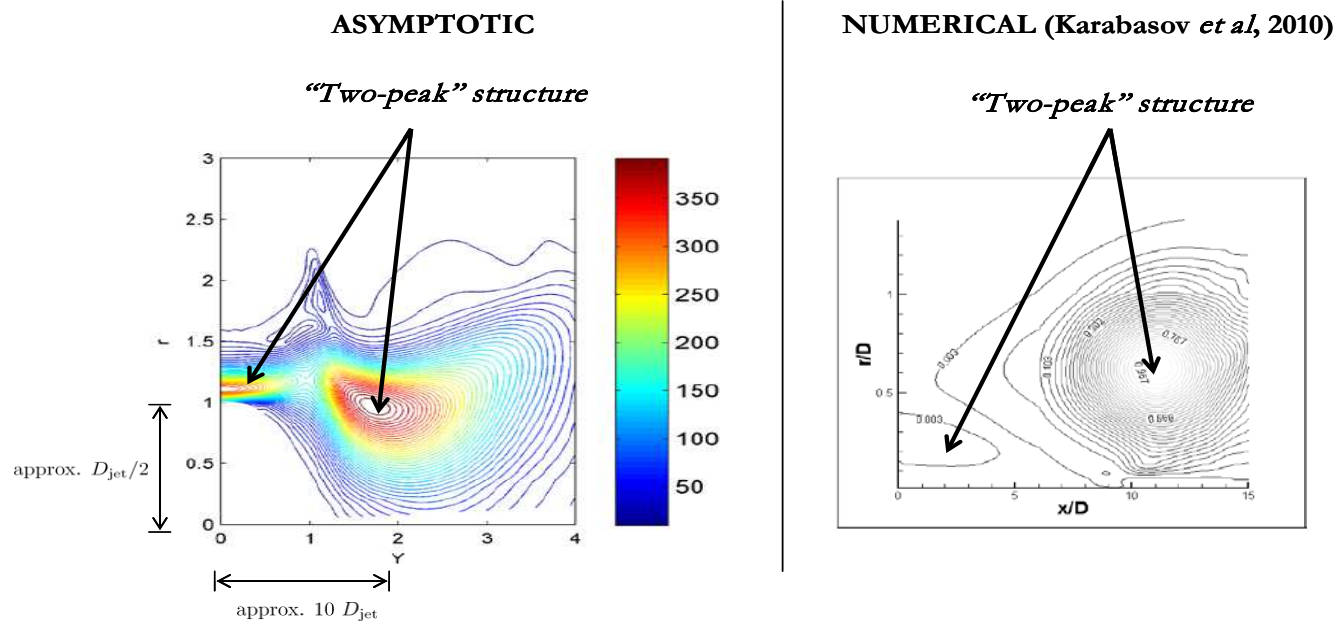


Figure 24. Comparison with Karabasov et al (2011)

The Karabasov *et al* (2011) results also show that the nonparallel flow doesn't affect the  $90^\circ$  sound field at any frequency.

The present asymptotic approach provides considerable insight into the relevant physics of the non-parallel mean flow interactions and is expected to be complementary to the numerical computations of Karabasov *et al* (2010, 2011). G & L found that the numerical computation of the weakly non-parallel Green's function becomes particularly difficult at low frequencies. The present results can be used to alleviate that problem because the Fourier transforms (5.8) of the terms in the Green's function expansions (5.5) and (5.6) can be used as a direct replacement for the Fourier transformed Green's functions that appear in their noise prediction code—or, for that matter, in any similar RANS based noise prediction code. The Fourier transforms (5.8) can be calculated by solving the boundary value problem (5.31), (5.45), (5.48) and substituting the results into (5.27) and (5.55). The mean flow parameters  $b, h, U_c$  can be determined from the RANS solution..

Tam and Auriault (1998) use a different form of the adjoint Green's function equation to compute the acoustic radiation from a point source at a particular location in a non-parallel mean flow. Their results suggest that the low frequency sound will be relatively insensitive to nonparallel mean flow effects at subsonic Mach numbers. But their computations are based on the 4<sup>th</sup> component  $g_{44}^a$  of the adjoint vector Green's function while the present analysis shows that it is the radial derivative of the axial component that makes the dominant contribution to the propagator in the acoustic formula (2.4) and therefore, corresponds to the dominant source of the low frequency sound radiation at small angles to the downstream axis. The present calculations also show that the derived

function  $\bar{v}$ , which roughly corresponds to  $g_{44}^a$ , is relatively insensitive to non-parallel flow effects except where critical layer effects come into play at the supersonic Mach numbers--as predicted by Tam and Auriault (1998). But the present calculations also show that the radial derivative  $\partial g_{14}^a / \partial r$  of the axial component of the Green's function can be strongly affected by nonparallel mean flow effects for certain source locations that lie in regions where the turbulence intensity is likely to be fairly high--suggesting that the low frequency sound will be strongly affected by nonparallel mean flow effects as found by Karabosov *et al* (2011).

### Acknowledgement

The authors gratefully acknowledge the support of the RANS Based Prediction element of NASA's supersonic fixed wing project and the Acoustics Jet noise Research element of NASA's subsonic fixed wing project. "A.S. is grateful to Dr. A. Afjeh for his financial support.

### APPENDIX A Possible Mean Flow

In this appendix we generalize the incompressible mean flow model given in Tam and Burton (1984) to a compressible flow with  $\tilde{c}^2$  determined from Crocco's Relation (5.33) by putting

$$\bar{\rho}U = \rho_c(Y)U_c(Y)e^{-(\ln 2)\Theta^2(Y,r)} \quad (\text{A.1})$$

where

$$\Theta(Y,r) = \begin{cases} 0, & r < h(Y) \\ [r - h(Y)]/b(Y), & r \geq h(Y) \end{cases}, \quad (\text{A.2})$$

$b(Y)$  denotes the width of the shear layer (or the jet radius) and  $h(Y)$  is the radial location of its inner boundary. It, then follows from the compressible continuity equation that

$$\begin{aligned} V_r = \frac{-1}{2r\rho} \left\{ \frac{\partial}{\partial Y} \rho_c(Y)U_c(Y) \left[ \frac{b^2(Y)}{\ln 2} (1 - e^{-(\ln 2)\Theta^2}) + \frac{h(Y)b(Y)}{\sqrt{\ln 2/\pi}} \operatorname{erf}(\sqrt{\ln 2}\Theta) \right] \right. \\ \left. + \rho_c(Y)U_c(Y) \frac{d}{dY} h^2(Y) \right\} \end{aligned} \quad (\text{A.3})$$

But

$$\bar{\rho}\tilde{c}^2 = \rho_\infty c_\infty^2 \quad (\text{A.4})$$

since the pressure is constant and (A.3) becomes

$$V_r = \frac{-\tilde{c}^2}{2r} \left\{ \frac{\partial U_c(Y)}{\partial Y} \frac{U_c(Y)}{\tilde{c}^2(Y)} \left[ \frac{b^2(Y)}{\ln 2} \left( 1 - e^{-(\ln 2)\Theta^2} \right) + \frac{h(Y)b(Y)}{(\ln 2/\pi)^{1/2}} \operatorname{erf} \left( (\ln 2)^{1/2} \Theta \right) \right] \right. \\ \left. + \frac{U_c(Y)}{\tilde{c}^2(Y)} \frac{d}{dY} h^2(Y) \right\} \quad (\text{A.5})$$

where  $\tilde{c}^2(Y)$  can be determined from the Crocco relation (5.33).

Solving (5.33), (A.1) and (A.4) for  $U$  shows that

$$U = \frac{2\alpha e^{-(\ln 2)\Theta^2}}{1 + \sqrt{1 + 2(\gamma - 1)\alpha^2 e^{-2(\ln 2)\Theta^2}}} \quad (\text{A.6})$$

where

$$\alpha \equiv U_c / \tilde{c}^2 \quad (\text{A.7})$$

And since conservation of momentum implies that

$$\int_0^\infty \rho U^2 r dr = \text{constant} \quad (\text{A.8})$$

this shows that

$$\int_0^\infty \rho U^2 r dr = \alpha^2 \int_h^\infty \frac{2e^{-2(\ln 2)\Theta^2}}{1 + \left[ 1 + 2(\gamma - 1)\alpha^2 e^{-2(\ln 2)\Theta^2} \right]^{1/2}} r dr + \frac{1}{2} \alpha^2 h^2 \\ = \frac{b^2 \alpha^2}{\ln 2} \int_0^1 \frac{2z}{1 + \sqrt{1 + 2(\gamma - 1)\alpha^2 z}} dz + h \alpha^2 \int_h^\infty \frac{2e^{-2(\ln 2)\Theta^2}}{1 + \sqrt{1 + 2(\gamma - 1)\alpha^2 e^{-2(\ln 2)\Theta^2}}} dr + \frac{1}{2} \alpha^2 h^2$$

$$= \frac{b^2}{(\gamma-1)\ln 2} \left\{ \frac{[2(\gamma-1)\alpha^2+1]^{3/2}-1}{3(\gamma-1)\alpha^2} - 1 \right\} + \frac{2hb\alpha^2}{\sqrt{2\ln 2}} \int_0^\infty \frac{e^{-z^2}}{1+\sqrt{1+2(\gamma-1)\alpha^2}e^{-z^2}} dz + \frac{1}{2}\alpha^2 h^2$$

= constant (A.9)

So

$$\frac{b^2}{(\gamma-1)\ln 2} \left\{ \frac{[2(\gamma-1)\alpha^2+1]^{3/2}-1}{3(\gamma-1)\alpha^2} - 1 \right\} = \text{constant} \quad (\text{A.10})$$

in the self similar region where  $h = 0$ ,

or

$$[2(\gamma-1)\alpha^2+1]^{3/2} - [1+3(\gamma-1)\alpha^2] = \text{constant} \frac{3(\gamma-1)\alpha^2}{b^2} \quad (\text{A.11})$$

These results depend on the three shear layer parameters  $b(Y)$ ,  $h(Y)$  and  $U_c$  and all computations in this paper are based on the distributions shown in figures A-1, A-2 and A-3.

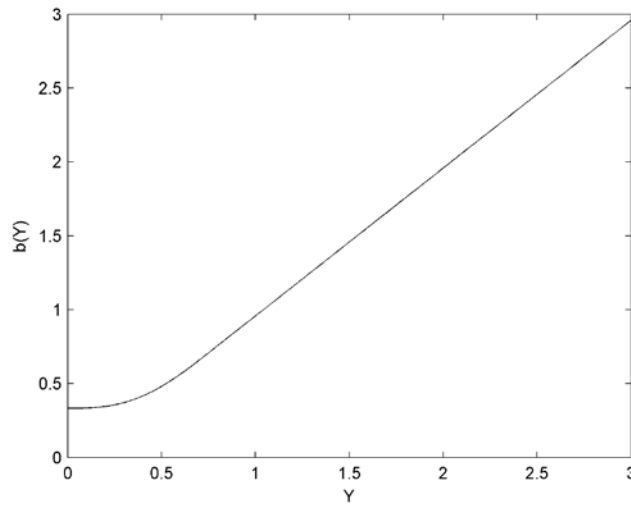


Figure A-1. Shear layer thickness parameter  $b$  as a function of  $Y$

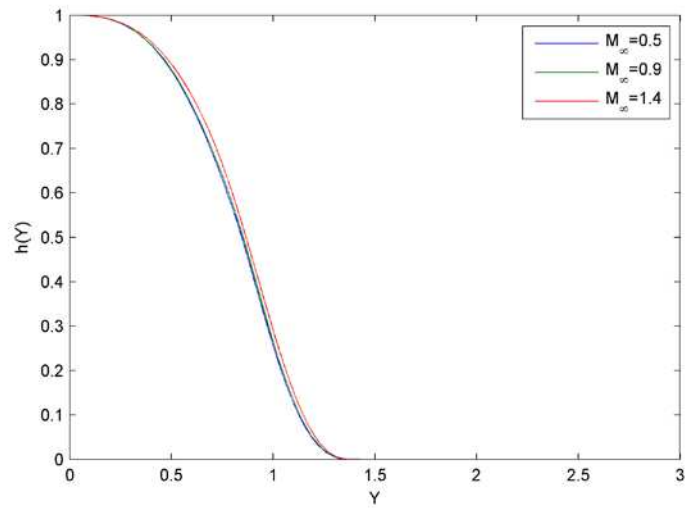


Figure A-2 Shear layer centerline location  $h$  computed from (A.9) for  $M_\infty = 0.5, 0.9, 1.4$ .

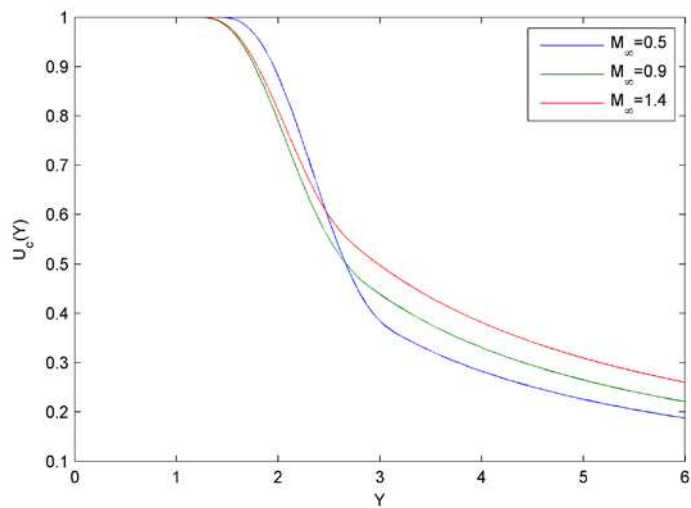


Figure A-3. Jet centerline velocity  $U_c$  with the downstream portion computed from (A.11) for  $M_\infty = 0.5, 0.9, 1.4$

**References**

Abramowitz, M. & Stegun, I. A., 1965, *Handbook of Mathematical Functions*, National Bureau of Standards, Washington

Afsar, M. Z. 2010 Asymptotic properties of the overall sound pressure level of sub-sonic air jets using isotropy as a paradigm. *J. Fluid Mech.*, 664, pp. 510-539.

Afsar, M. Z. 2011 *Insight into the two-source structure of the jet noise spectrum using a generalized shell model of turbulence. European Journal of Mechanics B/Fluids. Article in press.* [doi:10.1016/j.euromechflu.2011.06.002].

Bodony, D. J. & Lele, S. K., 2008, Low frequency sound sources in high-speed turbulent jets. *J. Fluid Mech.* **617**, 231 – 253.

Bogey, C & Bailly, C. 2010 The influence of nozzle-exit boundary layer conditions on the flow and acoustic fields of initially laminar jets. *J. Fluid Mech.* 663, pp. 507 – 540.

Crocco, L., 1932 Sulla transmission del calore da una lamina piana a un fluido scorrente ad alta velocita. *L'Aerotecnica*, 12, pp. 181-197. Translated as NACA TM 690

Freund, J., 2003, Noise source turbulence statistics and the noise from a Mach 0.9 jet. *Phys. Fluids*, 15, pp. 1788 – 1799.

Garabedian, P. R., 1964 *Partial Differential Equations*, John Wiley Publishers, New York, USA.

Goldstein, M. E. 1975 The low frequency sound from multipole sources in axisymmetric shear flows with application to jet noise. *J. Fluid Mech.* 70, pp.595-604.

Goldstein, M. E. 1976 The low frequency sound from multipole sources in axisymmetric shear flows with application to jet noise. Part 2. *J. Fluid Mech.* 75 part1, pp.17-28.

Goldstein, M. E. 2003. A generalized acoustic analogy. *J. Fluid Mech.* 488, pp. 315-333.

Goldstein, M.E. and Leib, S.J., 2008, The role of instability waves in predicting jet noise, *J. Fluid Mech.*, 525, pp.37-72.

Goldstein, M. E. 2006 Hybrid Reynolds-Averaged Navier-Stokes/Large Eddy Simulation Approach for Predicting Jet Noise, *AIAA J.* 44, No. 12 pp. 3136-3142

Goldstein, M. E. 2011, Recent developments in the application of the Generalized Acoustic Analogy to jet noise prediction, *International Journal of Aeroacoustics*, Vol10-No. 2 & 3, pp.89-116.

Goldstein, M.E. and Leib, S.J. 2008, “The Aero-acoustics of slowly diverging supersonic jets,” *J. Fluid Mech.*, 600, pp.291-337

Harper-Bourne, M., 2003, Jet noise measurements, AIAA 2003-3214.

Hirsch, C., 2001, Computational Methods for Inviscid and Viscous Flows, John Wiley and Sons,

ISBN-10: 0471924520.

Howe, M. S, 1970, Transmission of an acoustic pulse through a plane vortex sheet, *J. Fluid Mech.*), vol. 43, part 2, pp. 353-367

Karabasov, S. A., Hynes, T. P., Dowling, A. P. 2007 Effect of mean flow evolution on sound propagation through non-uniform mean flows, paper no. 2007-3655, 13<sup>th</sup> AIAA/CEAS Aero-acoustics Conference, Rome, Italy

Karabasov, S. A., Afsar, M. Z., Hynes, T. P., Dowling, A.P., McMullan, W. A., Pokora, C. D., Page, G. J., & McGuirk, J. J. 2008 Using Large Eddy Simulation within an Acoustic Analogy Approach for Jet Noise Modeling, paper no. 2008-2985, 14<sup>th</sup> AIAA/CEAS Aero-acoustics Conference, Vancouver, British Columbia, Canada.

Karabasov, S. A., Afsar, M. Z., Hynes, T. P., Dowling, A.P., McMullan, W. A., Pokora, C. D., Page, G. J., & McGuirk, J. J., 2010, Jet Noise: Acoustic Analogy Informed by Large Eddy Simulation, *AIAA Journal*, Vol. 48, No. 7, pp. 1312-1325

Karabasov, S. A. 2010 a Once again on the importance of propagation effects for jet noise modeling, AIAA paper # 2010-3966, 16<sup>th</sup> AIAA/CEAS Aero-acoustics Conference,

Karabasov, S. A. 2010 b Understanding Jet noise, *Phil. Trans. R. Soc. A* , vol. 368, pp. 3593-3608

Karabasov, S. A., Bogey, C & Hynes, T. P. 2011 Computation of noise of initially laminar jets using a statistical approach for the acoustic analogy: application and discussion, AIAA 2011-2929, 17<sup>th</sup> AIAA/CEAS Aero-acoustics conference Portland, Oregon.

Khavaran, A., Bridges, J. & Georgiadis, N., 2005, Prediction of turbulence-generated noise in unheated jets, NASA/TM 2005-213827.

Lighthill, M.J. 1952 On Sound Generated Aerodynamically: I. General Theory, *Proc. R. Soc. Lond., A* 211, pp. 564–587.

Lighthill, M. J. 1954 On sound generated aerodynamically: II. Turbulence as a source of sound, *Proc. R. Soc. Lond. A*, 222, pp. 1–32.

Lighthill, M. J. 1963, 'Jet noise'-The 1963 Wright Brothers Lecture, *AIAA Journal*, vol. 1, pp. 1507–1517.

Lilley, G. M. 1972 Generation of Sound in a Mixing Region, Lockheed Aircraft Co. 4<sup>th</sup> Monthly progress report on contract F-33615-71-C-1663, Marietta

McMullen, W. A., Pokora, C. D., Page, G. J., and McGuirk, J. J. 2008 Large eddy simulation of a high Reynolds number subsonic turbulent jet for acoustic source capture. AIAA 2008-2974. 14th Aeroacoustics conference, Vancouver, Canada.

Pokora, C. D & McGuirk, J. J. 2008, Spatio-temporal turbulence correlations using high speed PIV in an axi-symmetric jet. ,AIAA 2008-3028, 14<sup>th</sup> AIAA/CEAS Aero-acoustics conference, Vancouver. Sokolnikoff, I. S., & Redheffer, R. M. 1958 *Mathematics of Physics and Modern Engineering*, McGraw-Hill Book Company, Inc, New York, USA.

.Suzuky T. & Lele, S. K., *Green's functions for a source in a boundary layer: direct waves, channeled waves and diffracted waves*, *J. Fluid Mech.* (2003), vol. 477, pp. 129-173

Tam, C. K. W. & Burton, D. E, 1984, Sound generated by instability waves in supersonic flows, Part 2, *J. Fluid Mech.*, 138, pp. 273-295.

Tam, C. K. W. & Auriault, L., 1998, Mean flow refraction effects on sound from localized sources in a jet, *J. Fluid Mech.*, 370, pp. 149-174.

Tam, C. K. W., Viswanathan, K., Ahuja, K., and Panda, J. 2008 The sources of jet noise: experimental evidence. *J. Fluid Mech.*, 615, pp. 253 – 292.

Van Dyke, M., 1975, *Perturbation Methods in Fluid Mechanics*, The Parabolic Press, Stanford, California